Cellular Signalling 119 (2024) 111153

Contents lists available at ScienceDirect

Cellular Signalling

journal homepage: www.elsevier.com/locate/cellsig

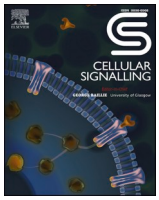

Computational modelling of dynamic cAMP responses to GPCR agonists for exploration of GLP-1R ligand effects in pancreatic β-cells and neurons

Lloyd Bridge [a,*], Shiqian Chen [b], Ben Jones [b]

[a] University of the West of England, Bristol, UK
[b] Imperial College, London, UK

ARTICLE INFO

Keywords:
GLP-1
Mathematical pharmacology
G protein-coupled receptors
Differential equations

ABSTRACT

The glucagon-like peptide-1 receptor (GLP-1R) is a class B G protein-coupled receptor (GPCR) which plays important physiological roles in insulin release and promoting fullness. GLP-1R agonists initiate cellular responses by cyclic AMP (cAMP) pathway signal transduction. Understanding of the potential of GLP-1R agonists in the treatment of type 2 diabetes may be advanced by considering the cAMP dynamics for agonists at GLP-1R in both pancreatic β-cells (important in insulin release) and neurons (important in appetite regulation). Receptor desensitisation in the cAMP pathway is known to be an important regulatory mechanism, with different ligands differentially promoting G protein activation and desensitisation. Here, we use mathematical modelling to quantify and understand experimentally obtained cAMP timecourses for two GLP-1R agonists, exendin-F1 (ExF1) and exendin-D3 (ExD3), which give markedly different signals in β-cells and neurons. We formulate an ordinary differential equation (ODE) model for the dynamics of cAMP signalling in response to G protein-coupled receptor (GPCR) ligands, encompassing ligand binding, receptor activation, G protein activation, desensitisation and second messenger generation. We validate our model initially by fitting to timecourse data for HEK293 cells, then proceed to parameterise the model for β-cells and neurons. Through numerical simulation and sensitivity studies, our analysis adds support to the hypothesis that ExF1 offers more potential glucose regulation benefit than ExD3 over long timescales via signalling in pancreatic β-cells, but that there is little difference between the two ligands in the potential appetite suppression effects offered via long-time signalling in neurons on the same timescales.

1. Introduction

G protein-coupled receptors (GPCRs) are cell surface receptors which are targets for up to 50% of all current drugs [1]. In recent years, analytical pharmacology has benefited from mathematical modelling approaches to answering questions regarding kinetic cellular responses to GPCR ligands [2–7]. Ordinary differential equation (ODE) models and simulation tools provide valuable insights into signalling pathway *dynamics* (beyond the limitations of equilibrium models, including the popular operational model of agonism [8]), while parameter estimation techniques applied to timecourse data sets allow quantification of kinetic ligand-receptor interaction parameters.

The glucagon-like peptide-1 receptor (GLP-1R) is a class B GPCR in the secretin receptor family. Important physiological actions of GLP-1R activation include stimulating the β-cells of the pancreas to release insulin, promoting satiety (fullness), and delaying nutrient absorption via slowing of gastric emptying [9]. Whilst the natural ligand for GLP-1R, GLP-1(7–36)NH_2, has a very short half-life of 2–3 min in the blood circulation, several stabilised analogues of GLP-1 have been developed by the pharmaceutical industry with extended pharmacokinetics [10]. In line with the physiological effects of native GLP-1, sustained GLP-1R activation by pharmaceutical GLP-1R agonists (GLP-1RAs) leads to weight loss via reduced energy intake and improves blood glucose levels by augmenting both insulin release and sensitivity. As such, approved GLP-1RAs such as exenatide, liraglutide, dulaglutide, semaglutide are commonly used to treat type 2 diabetes (T2D) and, in some cases, obesity. The main side effect of GLP-1RAs is nausea, which results from activation of specific neuronal populations in the brain stem [11].

As a primarily Gαs-coupled GPCR, GLP-1R signals principally via cyclic AMP [12]. It is also subject to desensitisation by recruitment of β-arrestins and undergoes rapid agonist-induced internalisation, resulting in receptor downregulation by post-endocytic trafficking into lysosomes [13]. There has been much interest in the prospect of modulating GLP-1R pharmacology via "biased agonism"; specifically, there is

* Corresponding author.
E-mail address: lloyd.bridge@uwe.ac.uk (L. Bridge).

https://doi.org/10.1016/j.cellsig.2024.111153
Received 24 January 2024; Received in revised form 19 March 2024; Accepted 26 March 2024
Available online 30 March 2024

evidence that GLP-1RAs with reduced tendency to recruit β-arrestins, but maintained cAMP signalling, will be able to continue actively signalling for longer. Several "G protein-biased" GLP-1RAs have been described in the preclinical literature, and there appears to be evidence that these ligands demonstrate enhanced therapeutic efficacy compared to non-biased comparators [14–16]. The situation in humans is less clear, but more recently developed agents including tirzepatide (approved) and orforglipron (in phase 3 trials) show pronounced G protein-biased GLP-1R agonism and appear to be highly therapeutically effective [17,18].

Interestingly, many G protein-biased GLP-1RAs are also partial agonists for G protein signalling [17–19]. Thus, they show reduced efficacy in general, but with the β-arrestin response more dramatically affected, so that G protein effects are, in comparison, favoured. Surprisingly, little attention has been paid to the potential impact of partial agonism on how these agonists act in different tissues. Partial agonist signalling is well known to be heavily modulated by differences in receptor density, which may differ greatly in different cell types. In this case, pancreatic β-cells express high levels of GLP-1R, whereas appetite regulatory neurons tend to express much lower levels [20,21]. Numerous other differences in the cell-specific proteome are poised to modulate how GLP-1R signalling is regulated.

With this in mind, we conducted experiments and simulations to assess differences in how two prototypical and oppositely biased GLP-1RAs, termed exendin-F1 (ExF1) and exendin-D3 (ExD3) [15], signal in primary tissues involved in mediating their physiological effects, namely, insulin-producing pancreatic β-cells and anorectic neurons from the nodose ganglion of the vagus nerve. ExF1 and ExD3 are peptide ligands derived from the prototypical GLP-1R agonist exendin-4, but with single amino acid substitutions at or close to the N-terminus (H1F or E3D). Our previous data show that ExF1, compared to ExD3, shows markedly reduced ability to recruit β-arrestin to the GLP-1R, and is also a partial agonist for Gαs signalling. In the present work we provide experimental data showing how these pharmacological differences translate to cAMP signalling dynamics in physiologically relevant cell types that endogenously express GLP-1R. We find that in β cells, the peak cAMP response to both ligands is similar, but that there is a more pronounced drop off in signal for ExD3. In neurons, the peak response is lower with ExF1, but for long times the signals for ExF1 and ExD3 converge.

We aim to understand and quantify the signalling dynamics by mathematical modelling of signal transduction via the GLP-1R, using a model comprising ligand binding, receptor and G protein activation, receptor desensitisation and production of the second messenger cAMP. This new model allows us to assess the differences in ExD3- and ExF1-driven signalling, paying attention to the potential roles of receptor activation and desensitisation from ligand-receptor complexes in β-cells and neurons.

The remainder of this paper is organised as follows. In Section 2 we formulate an ODE model for cAMP signalling comprising ligand binding, receptor and G protein activation, desensitisation and cAMP production. In Section 3, we use experimental data obtained using HEK293 cells to parameterise the model, giving an initial validation of the model and estimates for ligand on and off rates. In Section 4, we further validate and parameterise the model using experimental data for β-cells and neurons. In Section 5, we use the model to predict the signalling behaviour beyond the duration of the time-limited experiments, and provide insights into the system's sensitivity to key parameters under parameter regimes specific to each of the two ligands in each of the two cells. We conclude in Section 6 with a discussion of our main results and their potential significance.

2. Model formulation and numerical solution method

Our mathematical model comprises an ordinary differential equation (ODE) system which will be used to simulate the dynamics of intracellular cAMP in response to ligands binding at GLP-1R. The key components of this model are ligand-receptor binding, receptor activation and the G protein cycle (based on [2–4,22]), receptor desensitisation (based on [23]), and production of cAMP catalysed by active $G_\alpha GTP$ [3], followed by cAMP degradation.

A reaction scheme schematic for our model is shown in Fig. 1. The receptor is assumed to be able to exist either in an inactive or active state (R or R^* respectively). We use L and G to denote ligand and G protein respectively. For example, RG represents G protein-bound inactive receptor, LR^*G represents ligand-bound, G protein-bound active receptor, and so on. There are eight receptor states within the cubic ternary complex schema for activation of receptor from inactive state R to active state R^*, with coupling to G protein G and binding by ligand L (which is assumed to be supplied in such a way that its concentration is constant) [4]. In Fig. 1, the equilibrium rate constants $K_\bullet$ and cooperativity factors μ, ν, ζ are labelled on each reversible reaction. For the individual kinetic rate constants and factors, we use lower case k, and subscripts $+$ and $-$ to denote the forward and backward reactions respectively. Descriptions of the equilibrium rate constants and cooperativity factors for the cubic schematic are given in Table 1.

Desensitisation of receptor is incorporated into the model as in [23], with desensitised receptor species denoted R_{DS} and LR_{DS}. Ligand-bound active receptor LR^* becomes desensitised in a one-way reaction. The desensitised, inactive ligand-receptor complex may then reversibly dissociate. This process is summarised in the following reaction scheme:

$$LR^* \overset{k_{DS}}{\rightarrow} LR_{DS} \underset{\delta_+ k_{L+}}{\overset{\delta_- k_{L-}}{\rightleftharpoons}} R_{DS} + L, \tag{2.1}$$

where δ_+ and δ_- measure the change in propensity for ligand binding and dissociation, respectively, for desensitised receptor over non-desensitised receptor.

The G protein cycle follows from dissociation of R^*G and LR^*G complexes, with $\beta\gamma$, α_{GDP} and α_{GTP} being the dissociated G protein subunit species. The model incorporates the following reactions (see [4]):

$$R^*G \overset{k_{GTP+}}{\rightarrow} R^* + \alpha_{GTP} + \beta\gamma, \quad LR^*G \xrightarrow{\nu_- k_{GTP+}} LR^* + \alpha_{GTP} + \beta\gamma, \tag{2.2a}$$

$$\alpha_{GTP} \underset{k_{hyd-}}{\overset{k_{hyd+}}{\rightleftharpoons}} \alpha_{GDP}, \qquad \alpha_{GDP} + \beta\gamma \underset{k_{RA-}}{\overset{k_{RA+}}{\rightleftharpoons}} G. \tag{2.2b}$$

Here, α_{GTP} is the active signalling molecule.

Production of the intracellular second messenger cAMP is catalysed by α_{GTP} via a linear model (see [3]), with removal of cAMP modelled as a first order degradation process (see (2.3o)).

Applying the law of mass action to each of the reactions yields a model system comprising 15 ordinary differential equations (ODEs), for the concentrations of each species. The ODE system is given in (2.3).

$$\frac{d[R]}{dt} = k_{L-}[LR] - k_{L+}[L][R] + k_{act-}[R^*] - k_{act+}[R] + k_{G-}[RG] - k_{G+}[R][G], \tag{2.3a}$$

$$\frac{d[R_{DS}]}{dt} = \delta_- k_{L-}[LR_{DS}] - \delta_+ k_{L+}[L][R_{DS}], \tag{2.3b}$$

$$\begin{aligned}\frac{d[R^*]}{dt} = {} & k_{act+}[R] - k_{act-}[R^*] + \zeta_- k_{L-}[LR^*] - \zeta_+ k_{L+}[L][R^*] \\ & + \mu_- k_{G-}[R^*G] - \mu_+ k_{G+}[R^*][G] + k_{GTP+}[R^*G],\end{aligned} \tag{2.3c}$$

$$\begin{aligned}\frac{d[LR]}{dt} = {} & k_{L+}[L][R] - k_{L-}[LR] + \zeta_- k_{act-}[LR^*] - \zeta_+ k_{act+}[LR] + \nu_- k_{G-}[LRG] \\ & - \nu_+ k_{G+}[LR][G],\end{aligned} \tag{2.3d}$$

$$\frac{d[LR_{DS}]}{dt} = k_{DS}[LR^*] - \delta_- k_{L-}[LR_{DS}] + \delta_+ k_{L+}[L][R_{DS}], \tag{2.3e}$$

$$\frac{d[LR^*]}{dt} = \zeta_+ k_{act+}[LR] - \zeta_- k_{act-}[LR^*] + \zeta_+ k_{L+}[L][R^*] - \zeta_- k_{L-}[LR^*] + \mu_- \nu_- k_{G-}[LR^*G] - \mu_+ \nu_+ k_{G+}[LR^*][G] + \theta_a \nu_- k_{GTP+}[LR^*G] - k_{DS}[LR^*], \tag{2.3f}$$

$$\frac{d[RG]}{dt} = k_{G+}[R][G] - k_{G-}[RG] + \nu_- k_{L-}[LRG] - \nu_+ k_{L+}[L][RG] + \mu_- k_{act-}[R^*G] - \mu_+ k_{act+}[RG], \tag{2.3g}$$

$$\frac{d[R^*G]}{dt} = \mu_+ k_{G+}[R^*][G] - \mu_- k_{G-}[R^*G] + \zeta_- \nu_- k_{L-}[LR^*G] - \zeta_+ \nu_+ k_{L+}[L][R^*G] + \mu_+ k_{act+}[RG] - \mu_- k_{act-}[R^*G] - k_{GTP+}[R^*G], \tag{2.3h}$$

$$\frac{d[LRG]}{dt} = \nu_+ k_{G+}[LR][G] - \nu_- k_{G-}[LRG] + \nu_+ k_{L+}[L][RG] - \nu_- k_{L-}[LRG] + \mu_- \zeta_- k_{act-}[LR^*G] - \mu_+ \zeta_+ k_{act+}[LRG], \tag{2.3i}$$

$$\frac{d[LR^*G]}{dt} = \mu_+ \nu_+ k_{G+}[LR^*][G] - \mu_- \nu_- k_{G-}[LR^*G] + \zeta_+ \nu_+ k_{L+}[L][R^*G] - \zeta_- \nu_- k_{L-}[LR^*G] + \mu_+ \zeta_+ k_{act+}[LRG] - \mu_- \zeta_- k_{act-}[LR^*G] - \theta_a \nu_- k_{GTP+}[LR^*G], \tag{2.3j}$$

$$\frac{d[G]}{dt} = k_{G-}[RG] - k_{G+}[R][G] + \nu_- k_{G-}[LRG] - \nu_+ k_{G+}[LR][G] + \mu_- k_{G-}[R^*G] - \mu_+ k_{G+}[R^*][G] + \mu_- \nu_- k_{G-}[LR^*G] - \mu_+ \nu_+ k_{G+}[LR^*][G] + k_{GRA+}[\alpha_{GDP}][\beta\gamma] - k_{GRA-}[G], \tag{2.3k}$$

$$\frac{d[\alpha_{GDP}]}{dt} = k_{hyd+}[\alpha_{GTP}] - k_{hyd-}[\alpha_{GDP}] + k_{GRA-}[G] - k_{GRA+}[\alpha_{GDP}][\beta\gamma], \tag{2.3l}$$

$$\frac{d[\beta\gamma]}{dt} = k_{GTP+}[R^*G] + \theta_a \nu_- k_{GTP+}[LR^*G] + k_{GRA-}[G] - k_{GRA+}[\alpha_{GDP}][\beta\gamma], \tag{2.3m}$$

$$\frac{d[\alpha_{GTP}]}{dt} = k_{GTP+}[R^*G] + \theta_a \nu_- k_{GTP+}[LR^*G] + k_{hyd-}[\alpha_{GDP}] - k_{hyd+}[\alpha_{GTP}], \tag{2.3n}$$

$$\frac{d[cAMP_i]}{dt} = k_{cAMP+}[\alpha_{GTP}] - k_{cAMP-}[cAMP_i]. \tag{2.3o}$$

2.1. Initial conditions, pre-equilibration and simulation

Initial conditions for the agonist-stimulated system are generated numerically by simulating a ligand-free ($[L] = 0$) system initially with $[R] = R_{tot}$ and $[G] = G_{tot}$ (so that all other concentrations are initially zero) until a steady-state is reached. The new initial conditions are then applied to the system with appropriate nonzero $[L]$. All numerical solutions are generated using MATLAB's built-in stiff ODE solver ode15s.

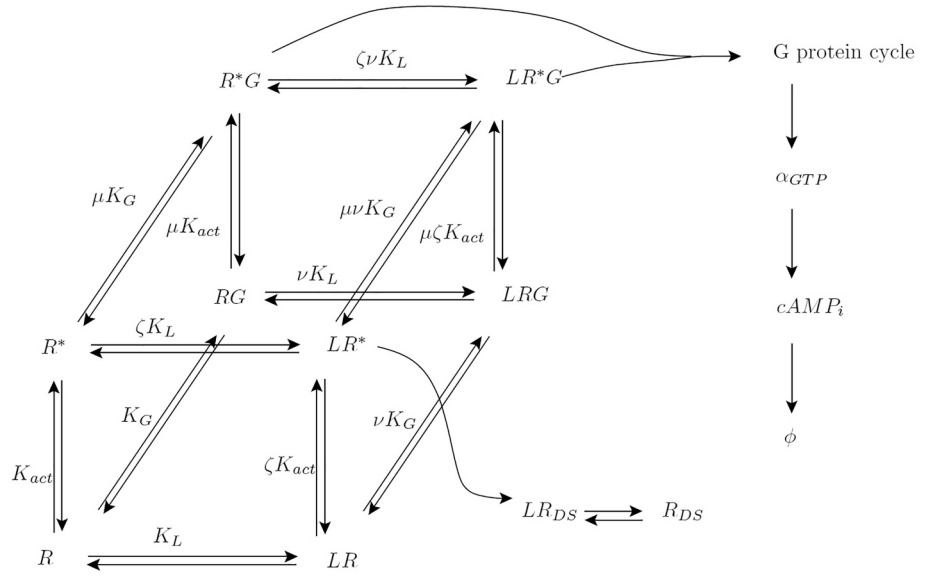

Fig. 1. The cubic ternary complex-based schematic, for ligand binding to, and activation of, receptor, with coupling to G protein. Equilibrium rate constants $K_\bullet$ and cooperativity factors μ, ν, ζ are labelled on each reversible reaction.

Table 1
Equilibrium rate constants and cooperativity factors for ligand/receptor/G protein interactions.

Label	Description of equilibrium constant
K_L	Association of ligand L and receptor R.
K_G	Binding of G protein G to receptor R.
K_{act}	Activation of receptor R to give active state R^*.
μ	Preference of G for R^* over R. Equally, the factor increase in propensity for $R \rightarrow R^*$ activation when R is G-bound.
ν	Preference of L for RG over R. Equally, the preference of G for LR over R.
ζ	Preference of L for R^* over R. Equally, the factor increase in propensity for $R \rightarrow R^*$ activation when R is L-bound.

3. Data fitting and parameterisation - HEK293 cells

As an initial model validation and parameterisation, we fit the model to timecourse data for cAMP responses to each of the two ligands of interest (ExF1 and ExD3) in HEK293 cells transfected with GLP-1R encoded in a BacMam vector. HEK293 cells are widely used throughout biological research. Here, the HEK293 data allow us to validate the model and estimate ligand on and off rates ahead prior to our analysis of the neuron and β-cell data sets. Full details of the cAMP dynamics response measurement are given in Appendix A.

Biosensor readouts which indicate second messenger levels may be calibrated to reflect conversion between biosensor response and concentrations. Such conversion is not always required to interpret signalling data [24], and biosensor readout traces are often used as proxies in the analysis of signalling kinetics (e.g., for cAMP) [25]. For simplicity here, we take

$$\text{measured signal} \quad S(t) = a[cAMP], \tag{3.1}$$

where a is a scaling factor specific to the experimental sensor. We note that biosensor calibration data, where available, may be used to fit to alternative nonlinear models [26]. Here we parameterise the ODE system by fitting to experimental data for cAMP response timecourses for the two different ligands, each in HEK293 cells with four different GLP-1R receptor expression levels (see Appendix A).

We estimate parameters by minimising the sum of squared errors between simulated timecourses and experimental data using the fminsearch optimisation routine in MATLAB. For each of the two ligands (ExF1 and ExD3), we estimate all system parameters including the four receptor levels, keeping all other parameters fixed across each of the receptor levels. Of particular interest are the on and off rate constants k_{L+} and k_{L-} for each ligand, and the receptor desensitisation rate constant k_{DS}.

In Fig. 2, we show the resulting fits to the eight timecourses (a timecourse for each of the four receptor concentrations, for each of the two ligands) given for $[L] = 1000$nM, noting the very good agreement. For each of the two ligands, the model captures the rise and fall nature of the cAMP response, on the correct timescales. ExD3 gives higher responses than ExF1, with greater curvature in the decay phase, which is captured by the model.

The estimated on and off rates, relative receptor concentrations and desensitisation rate constants are summarised in Table 2 and Fig. 3. The relative receptor levels are calculated as

Table 2
Fitted parameters for HEK293 cells.

Parameter	Units	Estimate from other experiment	Estimate using ExD3 data and current camp model	Estimate using ExF1 data and current camp model
ρ_1	–	0.258	0.385	0.169
ρ_2	–	0.938	1.256	1.113
ρ_3	–	12.4	7.486	16.32
ρ_4	–	100	100	100
k_{L+} (ExD3)	M^{-1} s^{-1}	1.512e+07	1.922e+07	–
k_{L-} (ExD3)	M^{-1} s^{-1}	0.01785	0.0134	–
k_{L+} (ExF1)	s^{-1}	1.718e+07	–	2.233e+07
k_{L-} (ExF1)	s^{-1}	0.2476	–	0.2485
k_{DS}	s^{-1}	–	3.475e-4	7.755e-06

$$\rho_i = \frac{R_{tot,i}}{R_{tot,max}} \times 100, \quad = 1, .., 4, \tag{3.2}$$

where $R_{tot,i}$ is the measured or estimated expression level for timecourse i, and $R_{tot,max}$ is the maximum receptor concentration. We note the good agreement between our fitted values and experimental estimates (obtained using binding assays and receptor expression experiments as described in Appendix A) for both the relative receptor concentrations in the plasma membrane and the on/off rates, providing a validation of the model. We also note that the estimated desensitisation rate constant k_{DS} is greater for ExD3 than for ExF1 in HEK293 cells.

We will use the fitted values of k_{L+} and k_{L-} when proceeding to fit to timecourse data for β-cells and neurons.

4. Data fitting and parameterisation - primary β-cells and neurons from mice

Here, we consider the cAMP dynamics of ExF1 and ExD3 in primary cells that 1) natively express GLP-1R and 2) are known to play an important role in GLP-1R-mediated physiological effects: nodose ganglion vagal neurons and pancreatic β-cells.

Cells were isolated from "CAMPER" mice expressing the cAMP sensor ^{T}Epac^{VV} to allow recording of cAMP responses by FRET microscopy. In Fig. 4, we show experimentally obtained cAMP timecourses in

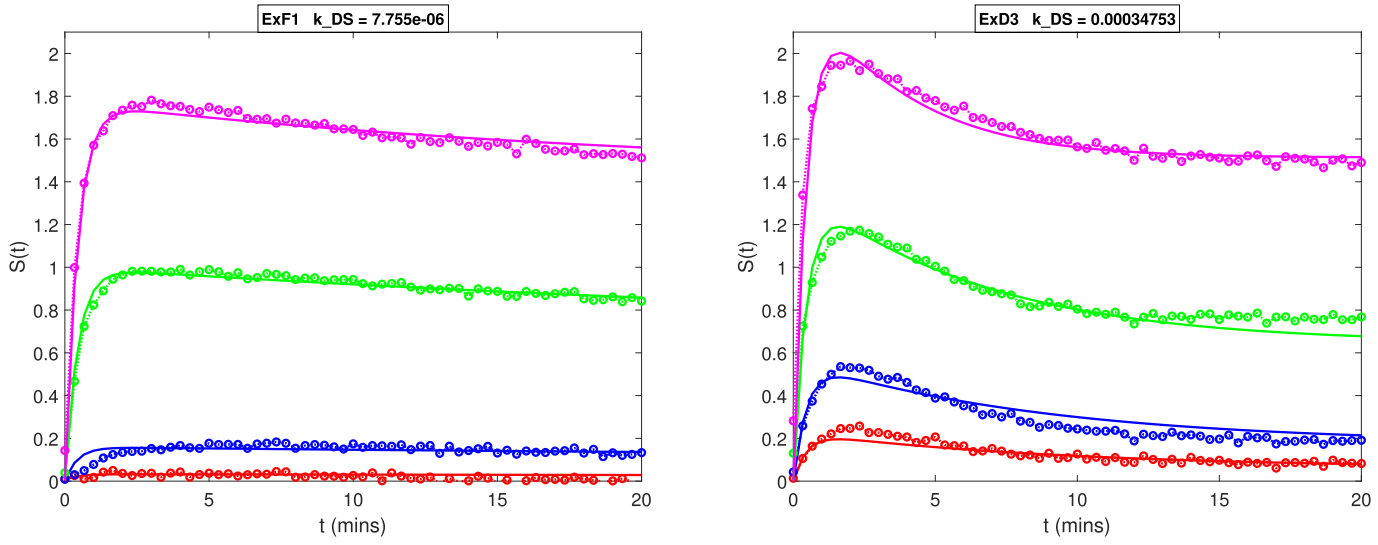

Fig. 2. Data fitting to timecourses for cAMP in response to 1000 nM ligand in HEK293 cells. Data points are in circles, and the fit is shown by a solid curve. The left-hand plot shows signal for ExF1, for four different receptor concentrations. The right-hand plot shows corresponding signal for ExD3.

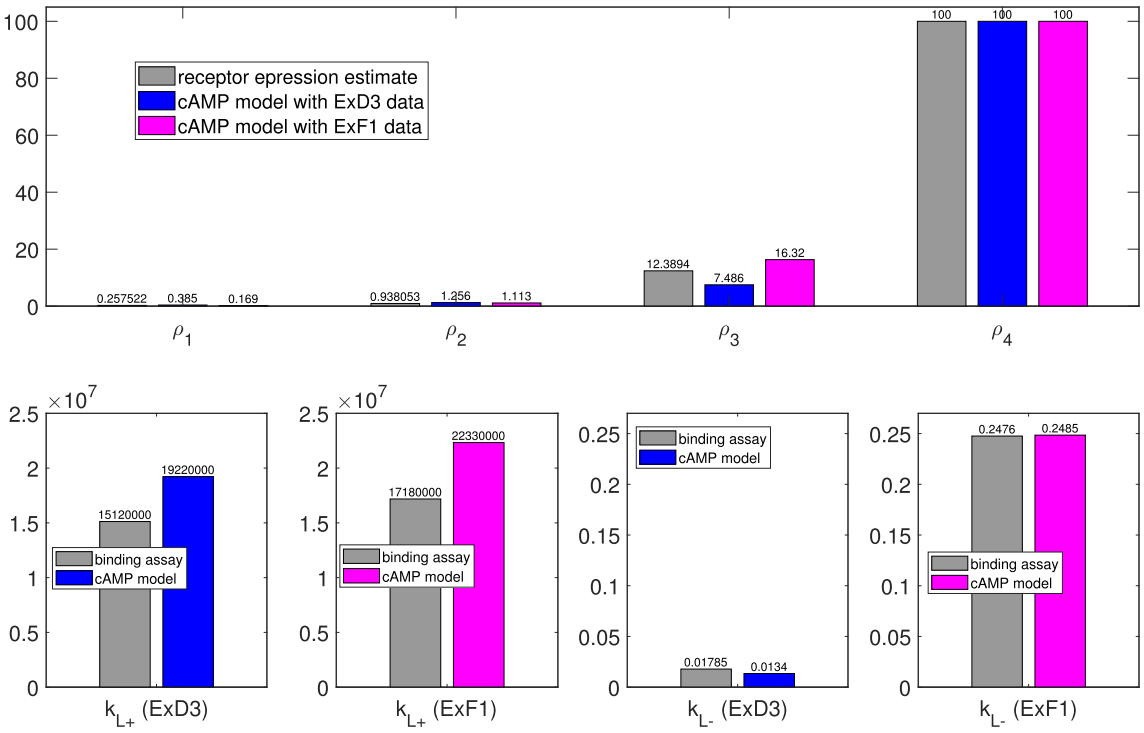

Fig. 3. HEK293 cell estimates given by fitting cAMP data to model (2.3), compared with estimates calculated by other means (see Appendix A). The estimates are summarised in Table 2.

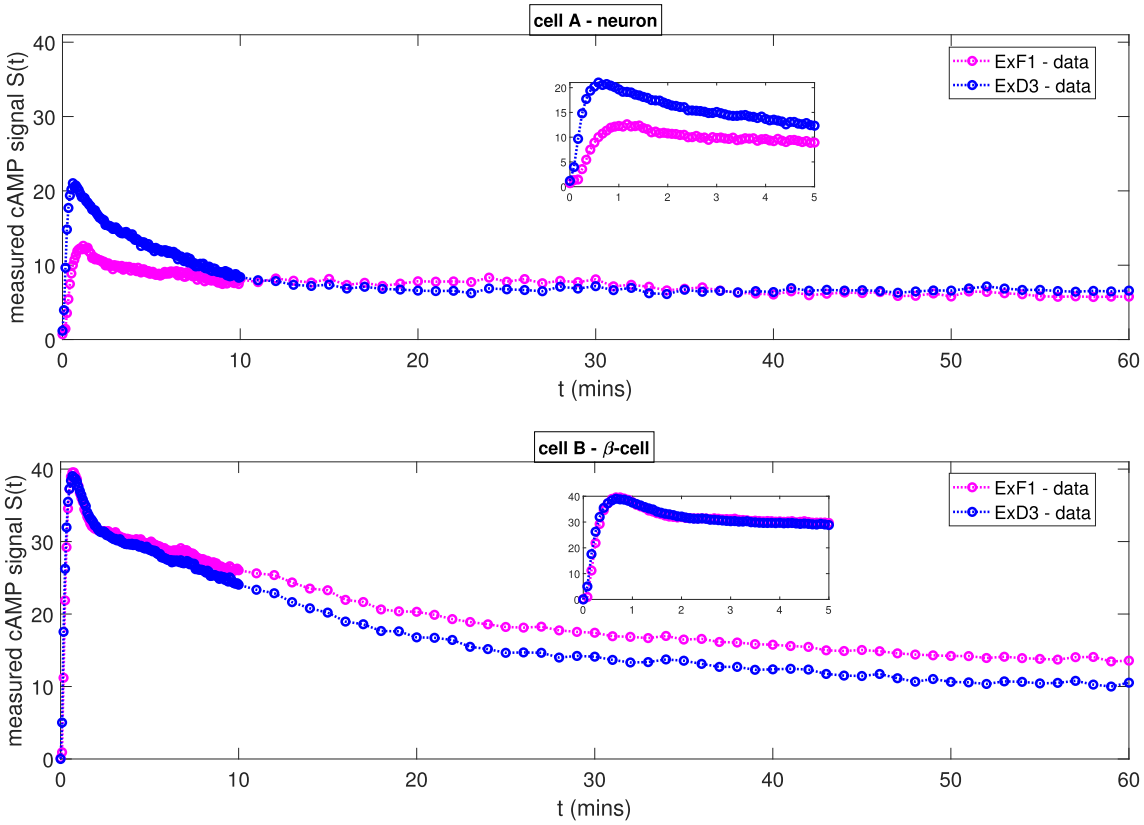

Fig. 4. cAMP timecourse data obtained using methods given in Appendix A, for two ligands (ExF1 and ExD3), each for two cell types (cell A - neuron, cell B - β-cell), with $[L] = 100$nM. Inset timecourses show first 5 min of response in detail.

response to 100 nM concentrations of each of the two ligands (ExF1 and ExD3), each for two further different cell types (cell A - nodose ganglion neuron, cell B - β-cell). Experimental details are given in Appendix A. For both ligands, the response is greater in β-cells. Each timecourse shows a clear rise-and-fall temporal profile with a peak response occurring on a timescale of one minute.

We now re-parameterise the system by fitting to the experimental data for cAMP timecourses for the two different ligands, each in β-cells and neurons. Again, we estimate parameters for minimising the sum of squared errors between simulated timecourse and experimental data using the fminsearch optimisation routine in MATLAB. For further validation of both the model and our findings so far, we fix the on and off rate constants (k_{L+} and k_{L-}) at the values estimated and tabulated in Table 2. We consider the scenario where on and off rate constants (k_{L+} and k_{L-}) and the ligand efficacy parameters $\zeta_{\pm}$ are ligand-specific, the rate constants and microaffinity constants pertaining to desensitisation of the LR^* complex (k_{DS}, $\delta_{\pm}$) are both ligand- and cell-specific, the microaffinity constants controlling the preference of L for RG over R ($\nu_{\pm}$) are both ligand- and cell-specific, and all other signalling parameters are cell-specific. Again, the experimental readout is given by

$$\text{measured signal} \quad = \quad a[cAMP], \tag{4.1}$$

where a is a scaling factor specific to the experimental sensor; as such, the estimated value of a is shared across all experiments, to which we fit the model simultaneously. Guided by published data indicating that GLP-1R expression is particularly high in β-cells in comparison to neurons [20], we additionally impose the constraint

$$R_{tot,B\ (\beta-\text{cell})} \ > \ R_{tot,A\ (\text{neuron})}. \tag{4.2}$$

In Fig. 5, we show the resulting fit to the four timecourses (a timecourse for each of the two ligands, in each of the two cells) given for $[L] = 100$nM, noting the excellent agreement. The estimated desensitisation rate constants are shown in Table 3 (the full estimated parameter set is tabulated in Appendix B). The model is clearly able to capture both the short-time and long-time behaviours. In neurons, ExD3 gives a higher response on the short ($\sim$ 5 mins) timescale, but there is little difference between the response for the two ligands on the longer timescale ($\sim$ 60 mins), over which the fitted responses appear to have reached an approximate steady-state. In β-cells, there is little difference between the response for the two ligands over the short ($\sim$ 5 mins) timescale, while ExF1 gives a higher response on the longer timescale ($\sim$ 60 mins), over which the response does not come to steady-state. For both cells, the desensitisation rate constant k_{DS} estimates are significantly higher for ExD3 than for ExF1. We also note that, for both ligands, the k_{DS} estimates are higher for neurons than for β-cells, although the difference is relatively small for ExD3.

Table 3
Fitted parameters for β-cell and neurons.

parameter	neuron	β-cell
k_{DS} (ExD3)	0.0018	6.341e-4
k_{DS} (ExF1)	1.299e-5	7.418e-07

We next proceed with several sensitivity analyses to explore the effects of key system parameters on cAMP responses.

5. Model predictions and sensitivity analysis

Using the estimated parameter values as our base values, we now consider the sensitivity of the simulated response to changes in model parameters (all figures in this section show model simulations). Base parameter values are given in Table 4.

5.1. Ligand concentration-response

We first examine the effect of ligand concentration $[L]$ on cAMP dynamics. Simulated timecourse curves for a range of ligand concentrations are shown in Fig. 6. We note that peak-plateau dynamics are apparent for the majority of the timecourses, consistent with the early peak response seen in the experimental data, and typical of theoretical GPCR activation profiles [4,25]. However, for some of the lower ligand concentrations, the cAMP signal is monotonic (so no peak), while for intermediate concentrations for the neuron-ExF1 simulations, peak-trough-plateau profiles are seen. There are clearly multiple phases (timescales) associated with the response.

Ligand concentration-response curves are shown in Fig. 7, summarising the first peak, maximum and long-time (60 min) cAMP responses over a range of ligand concentrations. A peak detection code searches for the first peak in the timecourse, and returns either that peak value if the

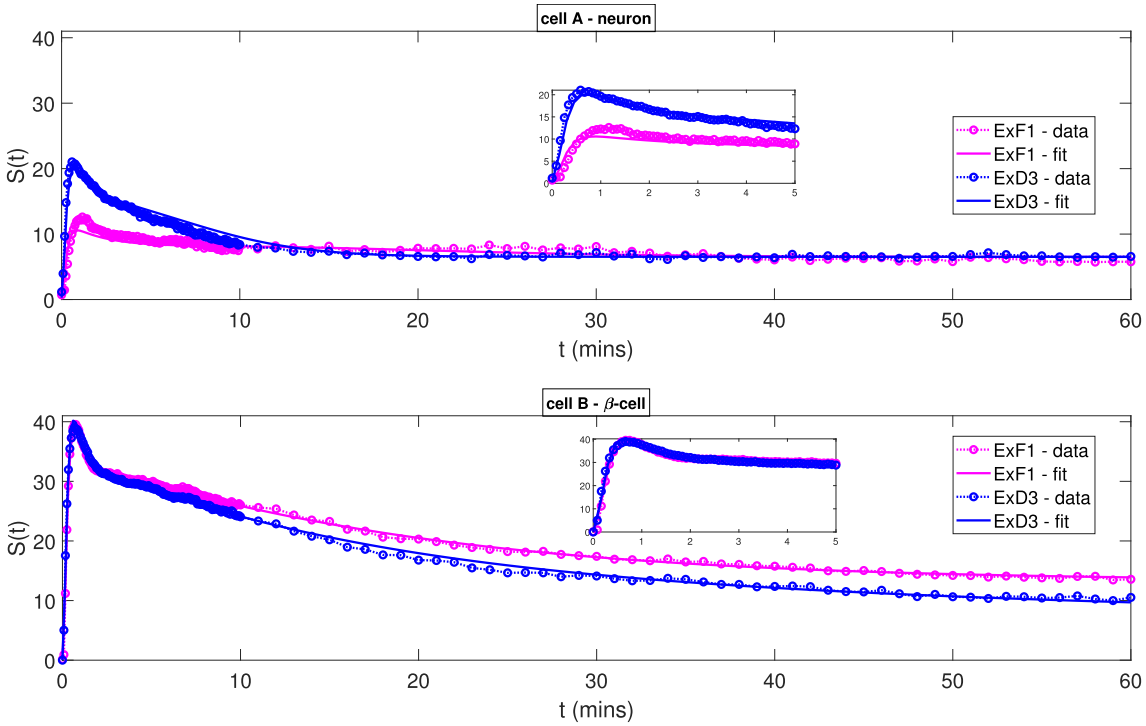

Fig. 5. Data fitting to timecourses for cAMP in response to 100 nM ligand in both neurons and β-cells.

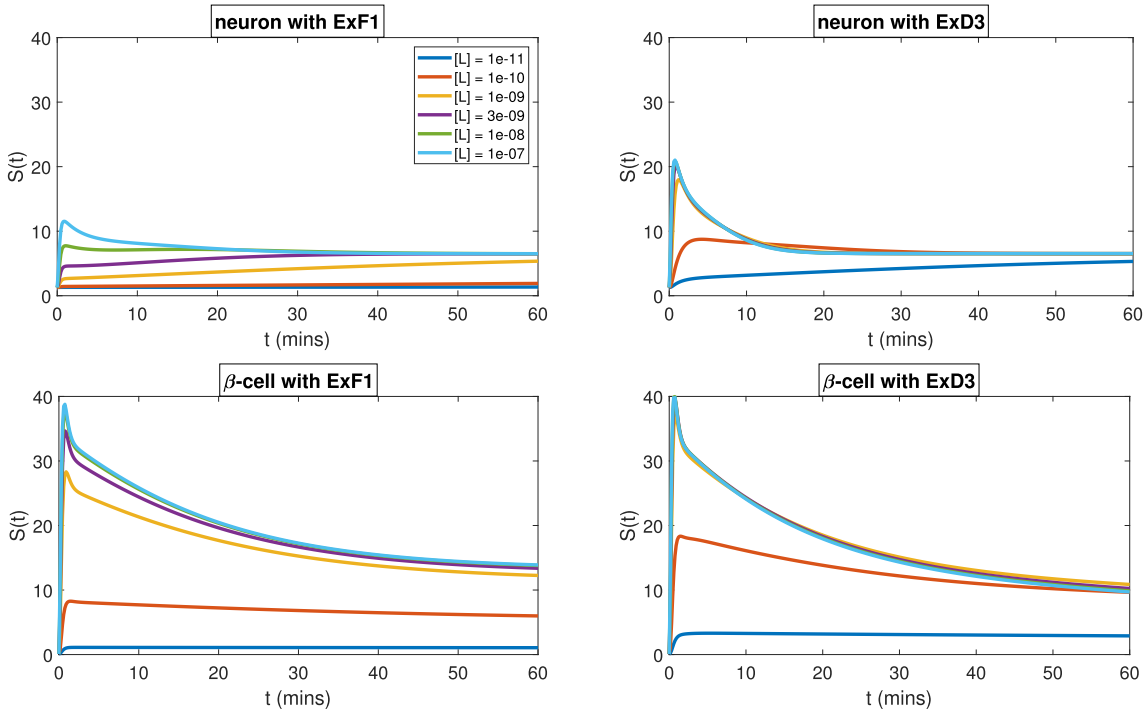

Fig. 6. Simulated timecourses for neurons and β-cells, for a range of ligand concentration $[L]$.

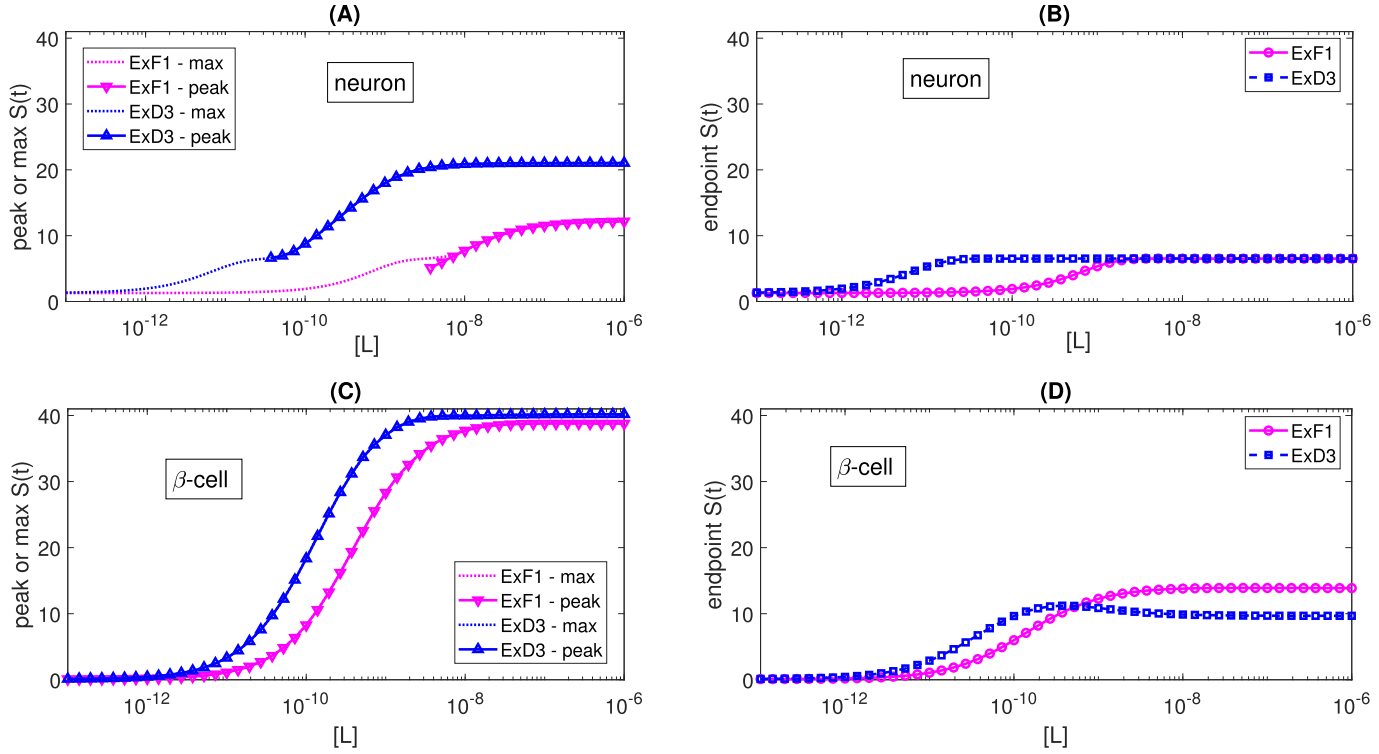

Fig. 7. Simulated ligand concentration-response curve for neurons and β-cells, for the first peak (if it exists), the maximum and long-time cAMP levels. The long-time result is for $t = 60$ mins. (A) First peak or maximum in neurons, (B) Endpoint signal in neurons, (C) First peak or maximum in β-cells, (D) Endpoint signal in β-cells.

first peak exists, or not-a-number if no peak exists. For neurons, there exists a range of ExF1 concentrations for which the first peak in the timecourse is not the maximum signal, again indicating multiphasic behaviour. For β-cells, the peak and maximum curves coincide.

From Figs. 6–7, we make further observations. The peak and maximum signal curves are monotonic for neurons for both ligands (Fig. 7(A)), and for β-cells for ExF1 (Fig. 7(C)). There is a slight overshoot (non-monotonicity) in the peak curve for ExD3 in β-cells (Fig. 7(C)). ExD3 gives a larger maximum response for both cell types, over the range of ligand concentrations. The endpoint curves are all non-monotonic (Fig. 7(B,D)), but this is only apparent by close inspection. The greatest relative overshoot is in the β-cell endpoint curve for ExD3

(Fig. 7(D)). ExD3 gives a larger endpoint response for low concentrations, but lower response at high concentrations. The endpoint response in neurons is very close for both ligands for $[L] > 10^{-9}$M, while the endpoint response in β-cells is higher for ExF1 than for ExD3, for $[L] > 10^{-9}$M. Finally, we note that the model predicts a greater level of constitutive activity for neurons than for β-cells.

5.2. Effect of total receptor

Receptor expression levels may be altered experimentally (see Appendix A), allowing the effect of total receptor on cAMP response to be explored. Here we generate simulated receptor concentration-response curves by varying R_{tot} over orders of magnitude for each cell type, for peak and endpoint signals in response to each of the two ligands.

In Fig. 8, we show the effect of varying R_{tot} on cAMP timecourses and their peak, maximum signal and endpoint (60 mins) signals. Simulations for a range of values of $R_{tot,A}$ are shown in the timecourses and the concentration-response curves. For neurons, the general trend is an increased signal with increased $R_{tot,A}$, with peak-plateau dynamics at high receptor concentrations and peak-trough-plateau dynamics at lower concentrations. The relative difference between the saturation level of the concentration-response curves for the two ligands is greater for the peak response than for the endpoint response. The peak response is more sensitive to changes in R_{tot} near the base estimated value than the endpoint value is. For neuron, ExD3 gives a higher response than the same concentration of ExF1.

The β-cell results in Fig. 8 show that increasing R_{tot} leads to an increased signal, except for some non-monotonicity in peak signal for high concentrations R_{tot}. There is little relative difference between the concentration-response curves for the two ligands for peak signal except for high concentrations R_{tot}. ExF1 now gives a higher response at endpoint, but a lower response for the peak. The cAMP responses in β-cells approach saturation at much higher values of R_{tot} than for neurons, and our concentration-response analysis suggests that receptor overexpression in β-cells may result in much higher transient cAMP responses.

We note that cAMP experiments that are run over a shorter timescale, and those that use a lower ligand concentration, yield more pronounced receptor concentration-response differences between the two ligands. Also, the endpoint response over a short timescale (for example, 5 min) will capture effects of the initial transient, giving non-monotonic receptor concentration-response curves. These effects are shown in Fig. 9, where a ligand concentration of 1 nM is used for a 5-min experiment.

5.3. Effect of desensitisation

Receptor desensitisation may play a significant role in the modulation of cAMP response [26]. The irreversible desensitisation model proposed in (2.1) will contribute to a decreased cAMP signal over time. In Fig. 10, we show the effect of varying the desensitisation rate constant k_{DS} (which is specific to both the cell type and the ligand) on cAMP timecourses and their peak and endpoint (60 mins) signals. The desensitisation effect is clear, in that the signal decreases as k_{DS} increases for both the peak and endpoint readouts. The peak is maintained over all simulations shown, and the relative decrease in peak signal is small compared to that for the endpoint signal. Furthermore, the desensitisation effect seems to be greater in β-cells; the relative change in both endpoint and peak signals across the range of k_{DS} shown is greater for β-cells than for neurons.

5.4. Longer experiments and rechallenge simulations

From Figs. 2–5, it is clear that the qualitative features of cAMP timecourses for both agonists ExF1 and ExD3 across the three cell types are similar. However, there are clear quantitative differences in the cAMP responses between the two cell types of interest (neuron and β-cell). In neurons, the peak cAMP response is lower with ExF1, but the endpoint (60 mins) response is similar for both ligands. In β-cells, the endpoint response is lower with ExD3, but the early response

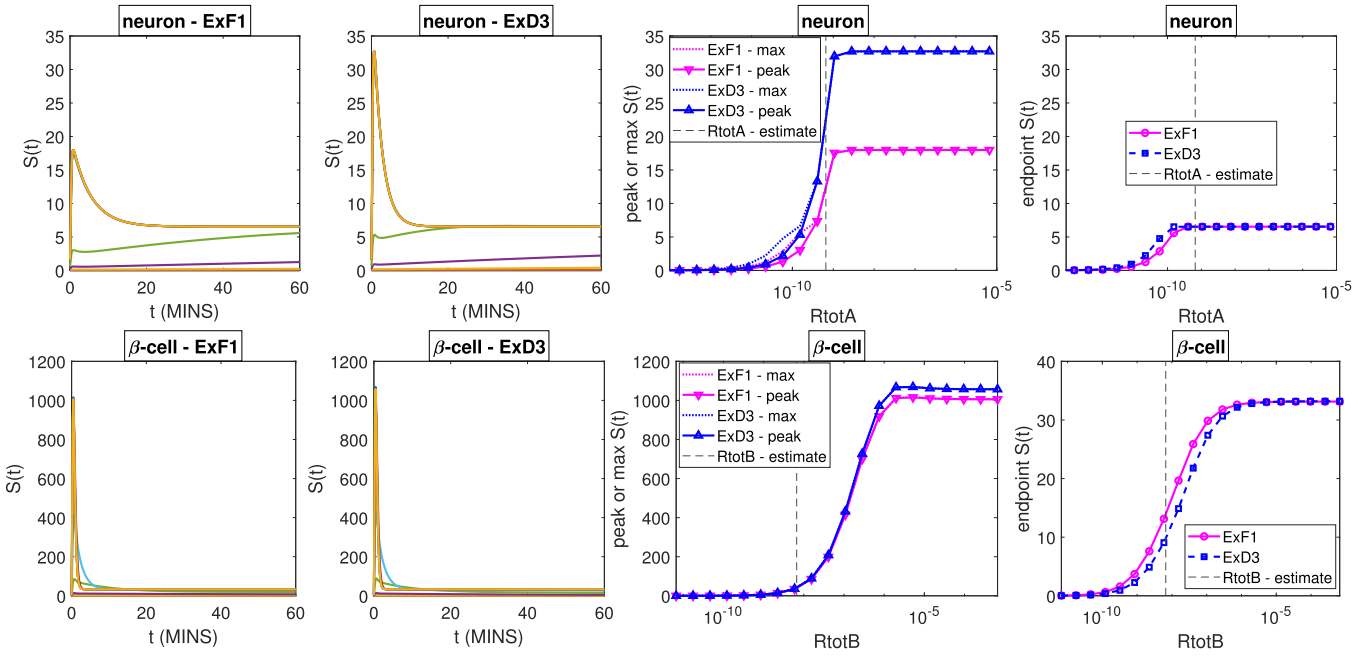

Fig. 8. Simulated effect of R_{tot} on cAMP response in both neurons and β-cells, for both ligands, each for ligand concentration $[L] = 100$nM. Top panel (neuron simulations) - cAMP response timecourses for both ligands, for a range of R_{tot}, followed by R_{tot} concentration-response curves for peak, maximum and endpoint (60 min) signals. Bottom panel (β-cell simulations) - as above. Dashed vertical lines in the concentration-response curves indicate the estimated value of R_{tot} from Fig. 5. Each coloured curve in the timecourse plots corresponds to a different value of R_{tot}.

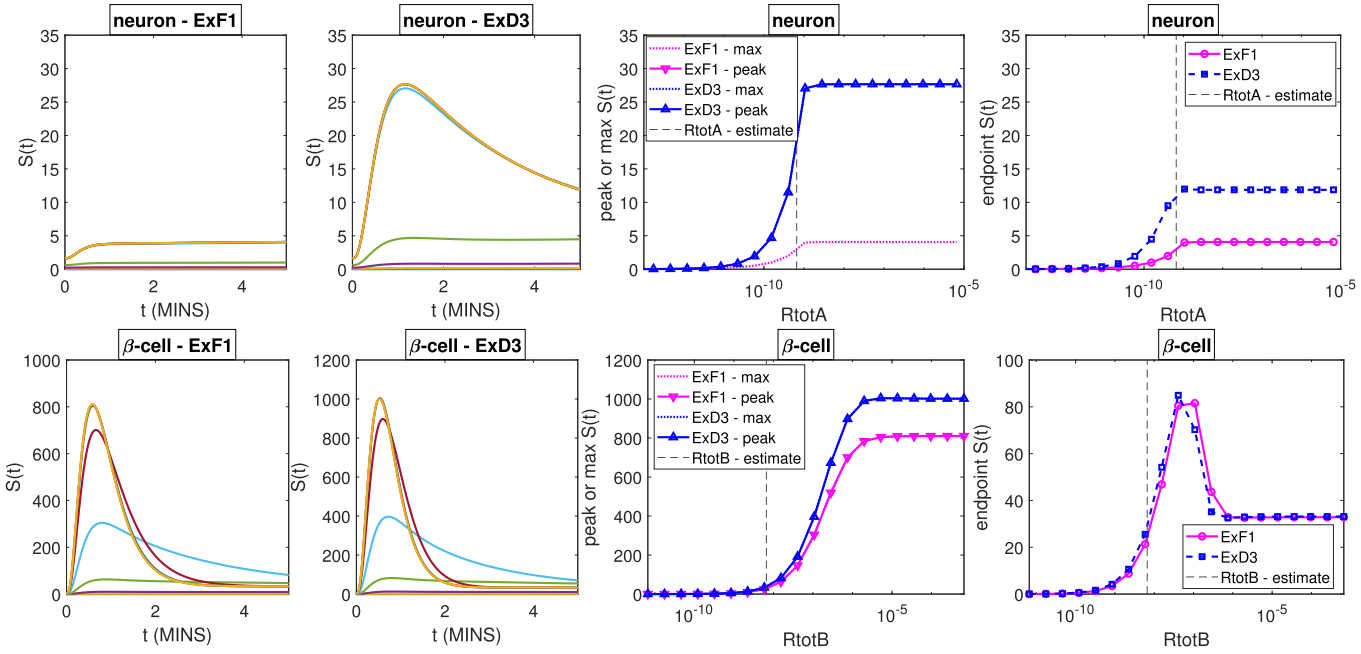

Fig. 9. Simulated effect of R_{tot} on cAMP response in both neurons and β-cells, for both ligands, each for ligand concentration $[L] = 1$nM. Top panel (neuron simulations) - cAMP response timecourses for both ligands, for a range of R_{tot}, followed by R_{tot} concentration-response curves for peak, maximum and endpoint (5 min) signals. Bottom panel (β-cell simulations) - as above. Dashed vertical lines in the concentration-response curves indicate the estimated value of R_{tot} from Fig. 5. Each coloured curve in the timecourse plots corresponds to a different value of R_{tot}.

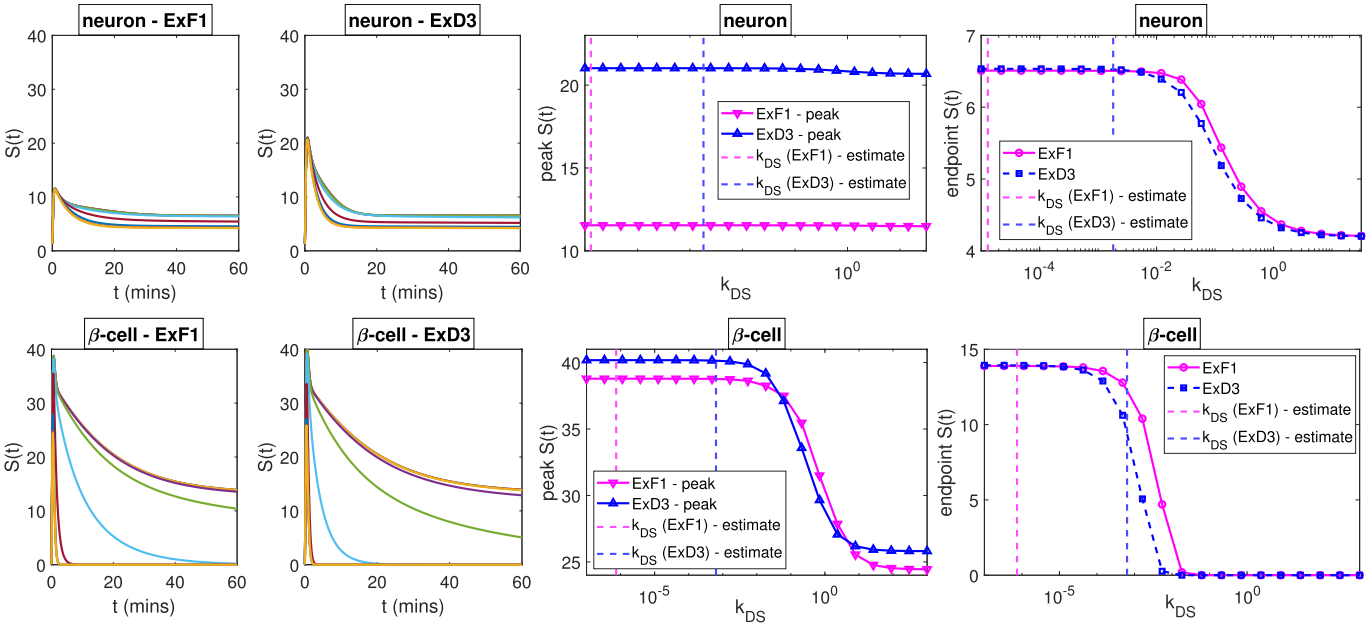

Fig. 10. Simulated effect of desensitisation rate constant k_{DS} on cAMP response in both neurons and β-cells, for both ligands, each for ligand concentration $[L] = 100$nM. Top panel (neuron simulations) - cAMP response timecourses for both ligands, for a range of k_{DS}, followed by k_{DS} parameter-response curves for peak and endpoint (60 min) signals. Bottom panel (β-cell simulations) - as above. Dashed vertical lines in the parameter-response curves indicate the estimated value of k_{DS} from Fig. 5. Each coloured curve in the timecourse plots corresponds to a different value of k_{DS}.

(incorporating the peak) is similar for both ligands. The cAMP dynamics differ quantitatively between the two cells. Our sensitivity analyses in Section 5 suggest that perturbing the system from the estimated parameters (in particular for k_{DS}) will yield responses which approach steady-states on different timescales. We wish to explore the approach to steady-state for the data shown in Fig. 5. The differing approaches to steady-state are difficult to assess by eye from the plotted data. The experimental data are limited, due to laboratory practicalities, to the first 60 min of cAMP response. However, we may, of course, generate timecourses beyond 60 min by simulation.

In Fig. 11, we show simulations beyond the 60 min of data used for fitting. In each case, we simulate cAMP response to agonist up to an endpoint time of 120 min or 480 min. It is now apparent that our model suggests that for neurons, the response has reached an apparent steady-

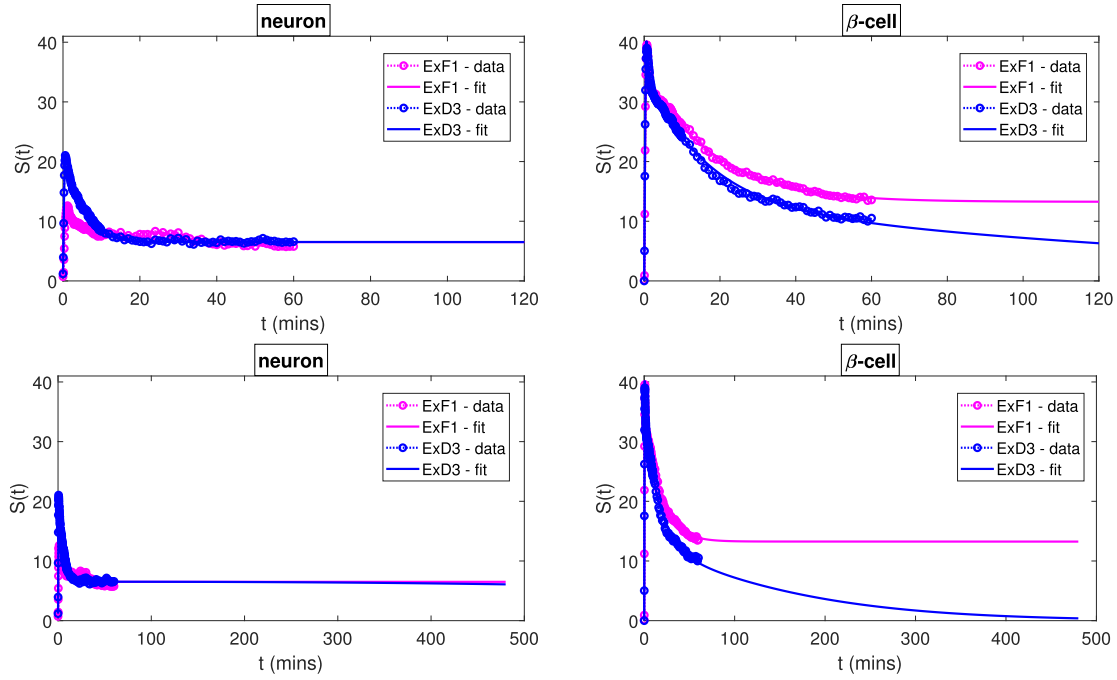

Fig. 11. Simulated response beyond 60 min, for $[L]$ = 100nM. Top panel - responses up to 120 min. Bottom panel - responses up to 8 h. Experimental data for the first 60 min are also shown.

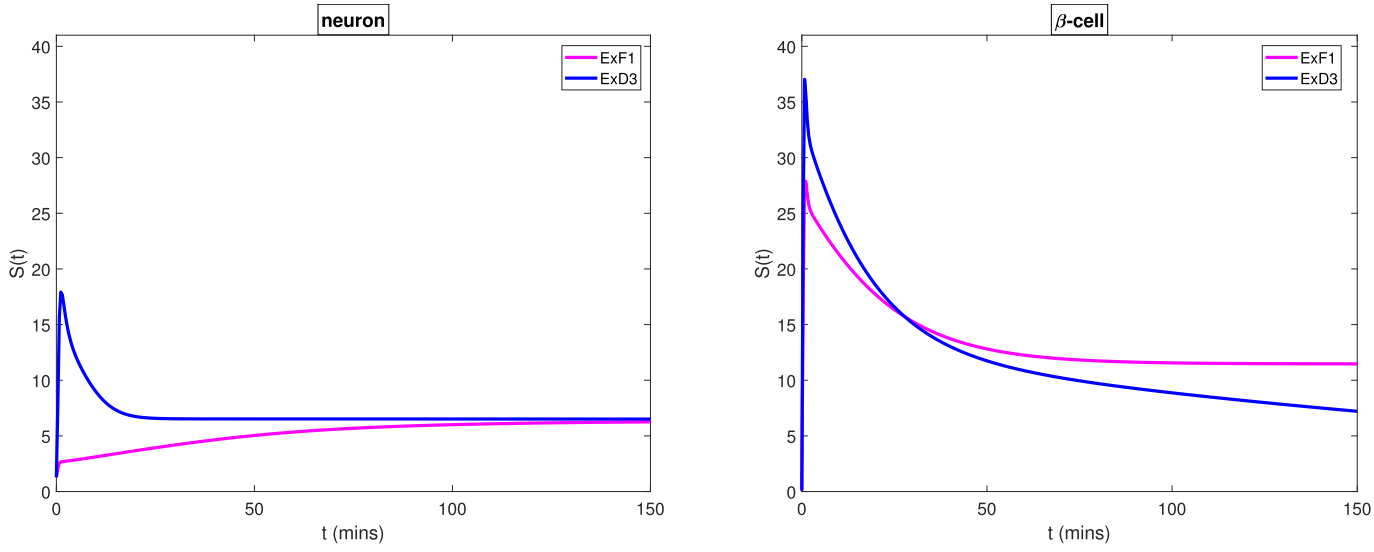

Fig. 12. Simulated response beyond 60 min, for $[L] = 1$ nM.

state already after 60 min. In contrast, for β-cells, the cAMP response continues to decay beyond 60 min, markedly for ExD3. The response to ExD3 is at around 1% of its initial value after 480 min. In Fig. 12, we show further simulated timecourses for a lower ligand concentration. We note that the model now predicts a crossover between the ExF1 and ExD3 timecourses for β-cells, with steady-state apparently reached for ExF1 by after 150 min, but the ExD3 response still decreasing. Again, the neuron response is lower, and now the neuron ExF1 response has lost its peak-plateau dynamics.

5.4.1. *Washout and re-challenge experiments*

A second "long-time" experimental analysis which may indicate differences in signalling dynamic profiles between the two ligands and the two cells concerns agonist re-challenge experiments. In such experiments, an initial "challenge" with ligand is followed by a ligand washout, and then a second challenge with the ligand [27,28]. A lower response from the second challenge may indicate a degree of receptor desensitisation.

In Fig. 13, we show simulations of washout and re-challenge experiments to demonstrate the potential effect of receptor desensitisation. In each case, we simulate cAMP signal $S(t)$ to agonist up to an endpoint time of 120 min, followed by the response as the ligand is washed off (modelled by setting $[L] = 0$) for 120 min, followed by the reintroduction of ligand at the same concentration for a final 120 min. For neurons, the cAMP response drops off by a relatively small amount during the washout phase, and the response to the rechallenge is

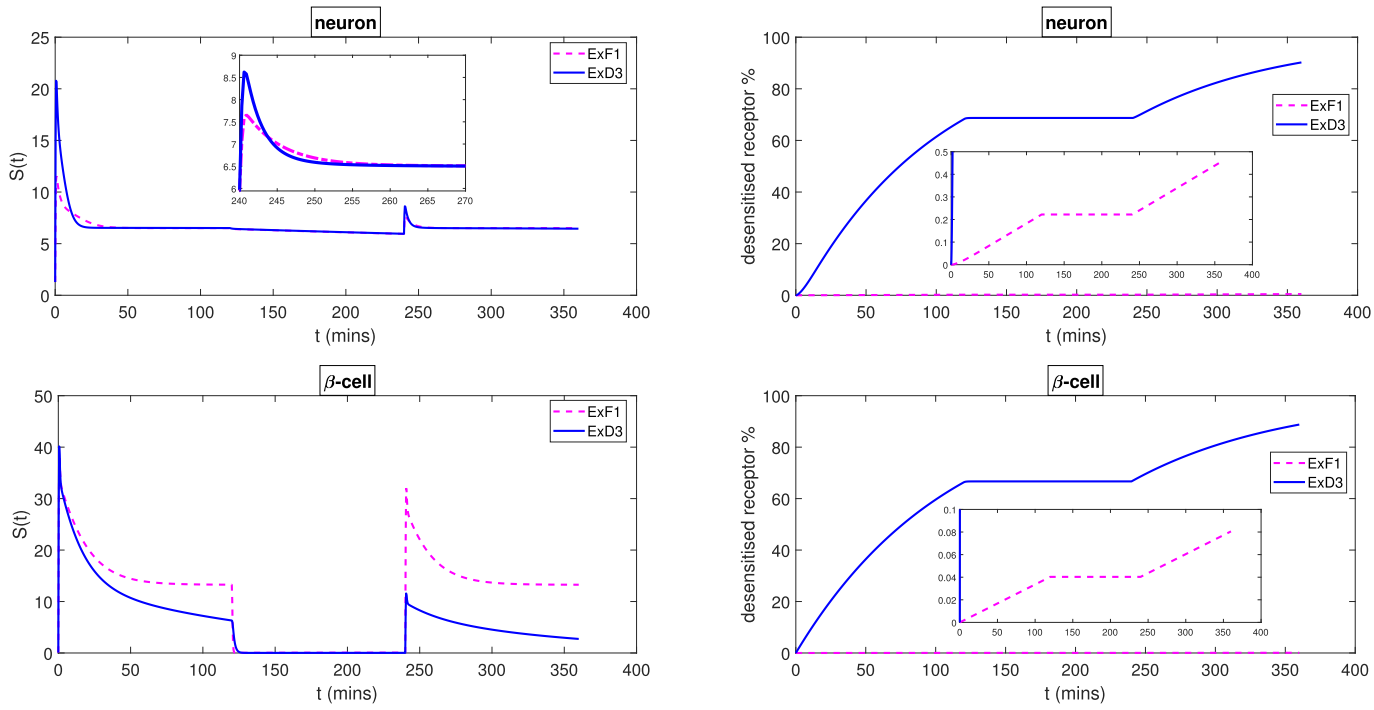

Fig. 13. Simulated timecourses of cAMP response in rechallenged β-cells and neurons. Simulations are for cAMP response to agonist (first 120 mins), followed by agonist washout (between 120 and 240 mins), followed by response to agonist again ("rechallenged" cells, with agonist after 240 mins). Right-hand panel shows percentage of total receptor that has been desensitised.

noticeable for both ligands. For β-cells, the drop-off in cAMP response during the washout phase is more rapid, and the cAMP response returns to almost zero. Also, the relative response to the rechallenge is larger than for neurons. In β-cells, the rechallenge response to ExF1 is larger than that for ExD3, indicating that ExD3-bound receptor may experience more significant desensitisation than ExF1-bound receptor in this case. In the right-hand panel of Fig. 13, we plot the percentage of receptor which has been desensitised, given by

$$\text{desensitised receptor}\% = 100\left(\frac{[R_{DS}] + [LR_{DS}]}{R_{tot}}\right) \tag{5.1}$$

It is clear that the desensitisation proceeds only while the ligand is present. Also, the proportion of receptor which is desensitised is much lower for ExF1 than for ExD3, as postulated from the cAMP timecourses.

Further insights may be gained from considering timecourses for each of the species in the model (2.3). In Figs. 14–15, we show the

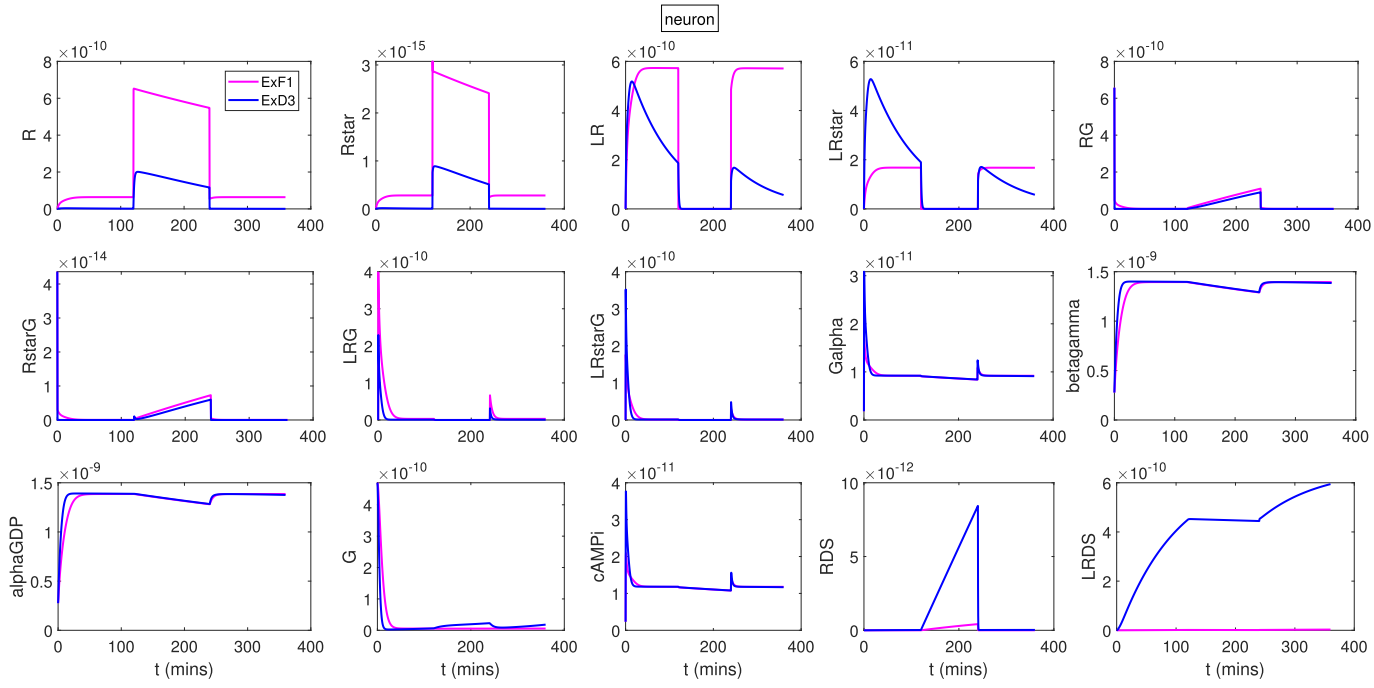

Fig. 14. Simulated timecourses of individual model species underlying the cAMP signal in neurons shown in Fig. 13.

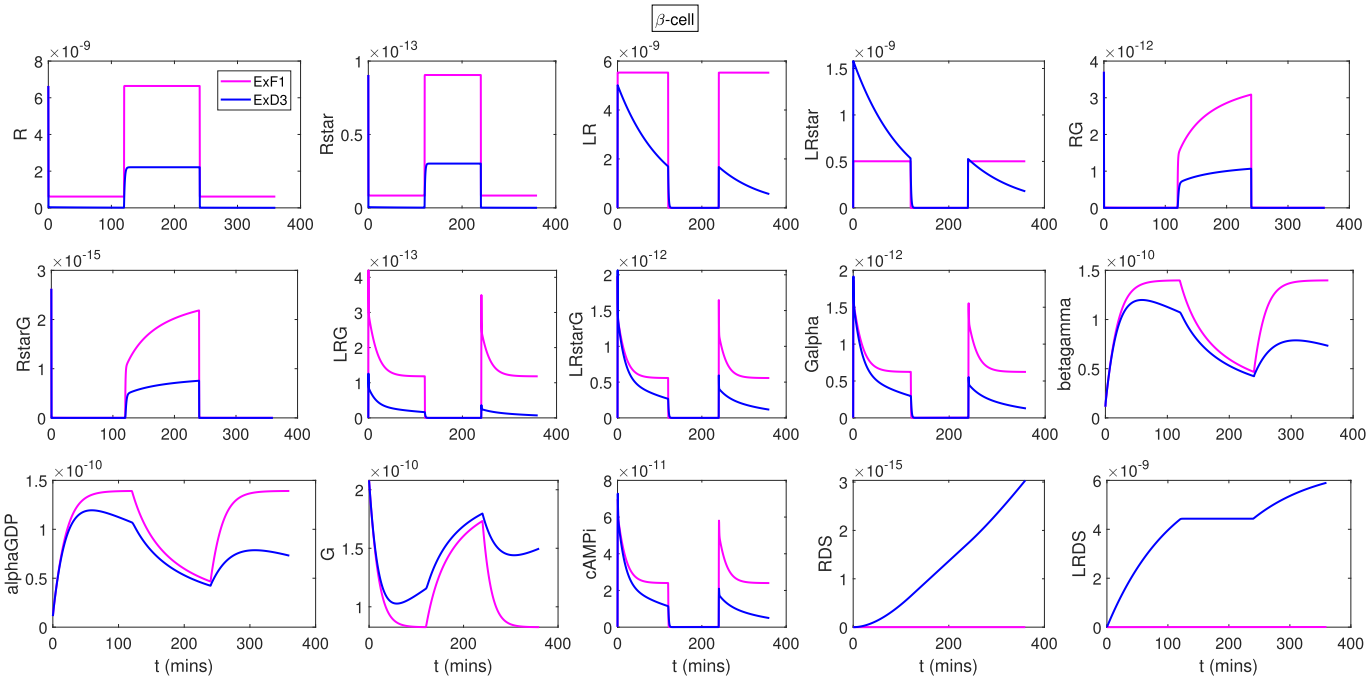

Fig. 15. Simulated timecourses of individual model species underlying the cAMP signal in β-cells shown in Fig. 13.

timecourses for each of the 15 species. The post-washout phases of the rechallenge experiments show similar signalling dynamics to the pre-washout challenge for ExF1. There is a marked difference, though, in the profiles for ExD3; the responses to the second ligand challenge generally do not reach the same levels as for the first challenge.

A final analysis shown in Fig. 16 considers the effect of the desensitisation rate constant k_{DS} on cAMP signal features. An interesting contrast to Fig. 10 is that the second peak disappears for large values of k_{DS}, even when the first peak still exists.

5.5. Effect of ligand efficacy

The cAMP response in our model varies according to a trade-off between receptor activation driving the G protein cycle and receptor desensitisation. In [23], this trade-off is analysed theoretically at the level of receptor activation with respect to changes in desensitisation and ligand efficacy parameters. We now consider the effect of the forward ligand efficacy parameter ζ_+ in our model.

In Fig. 17, we show the effect of varying the kinetic ligand efficacy

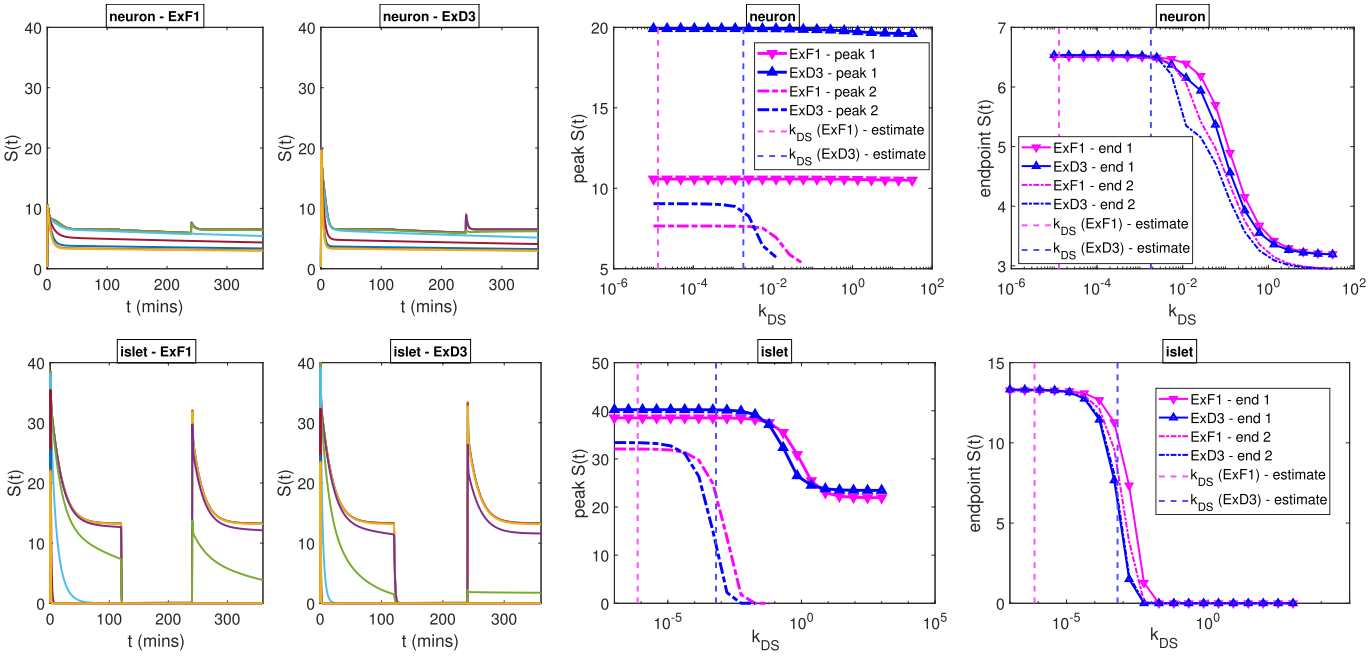

Fig. 16. Simulated effect of desensitisation rate constant k_{DS} on cAMP response in both neurons and β-cells, for both ligands, each for ligand concentration $[L]$ = 100nM, with washout and rechallenge. Top panel (neuron simulations) - cAMP response timecourses for both ligands, for a range of k_{DS}, followed by k_{DS} parameter-response curves for peak and endpoint (60 min) signals after both ligand challenges. Bottom panel (β-cell simulations) - as above. Dashed vertical lines in the parameter-response curves indicate the estimated value of k_{DS} from Fig. 5.

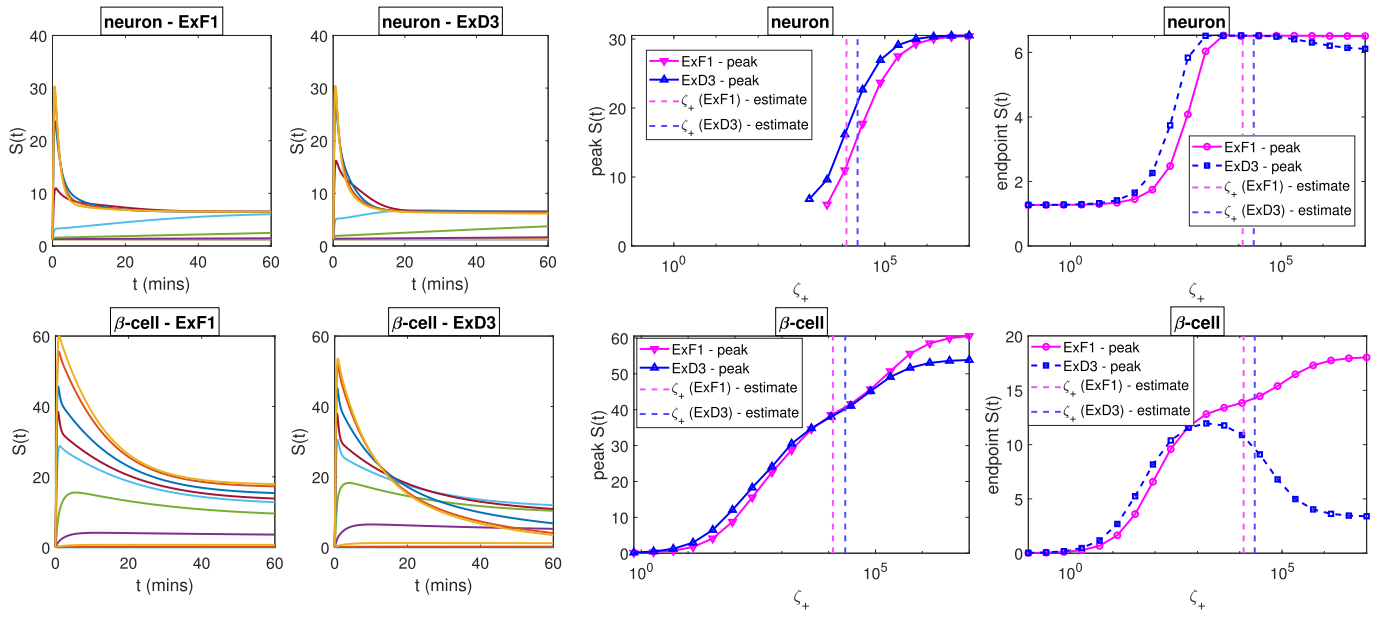

Fig. 17. Simulated effect of ligand efficacy parameter ζ_+ on cAMP response in both neurons and β-cells, for both ligands, each for ligand concentration $[L] = 100$nM. Top panel (neuron simulations) - cAMP response timecourses for both ligands, for a range of k_{DS}, followed by k_{DS} parameter-response curves for peak and endpoint (60 min) signals. Bottom panel (β-cell simulations) - as above. Dashed vertical lines in the parameter-response curves indicate the estimated value of ζ_+ from Fig. 5.

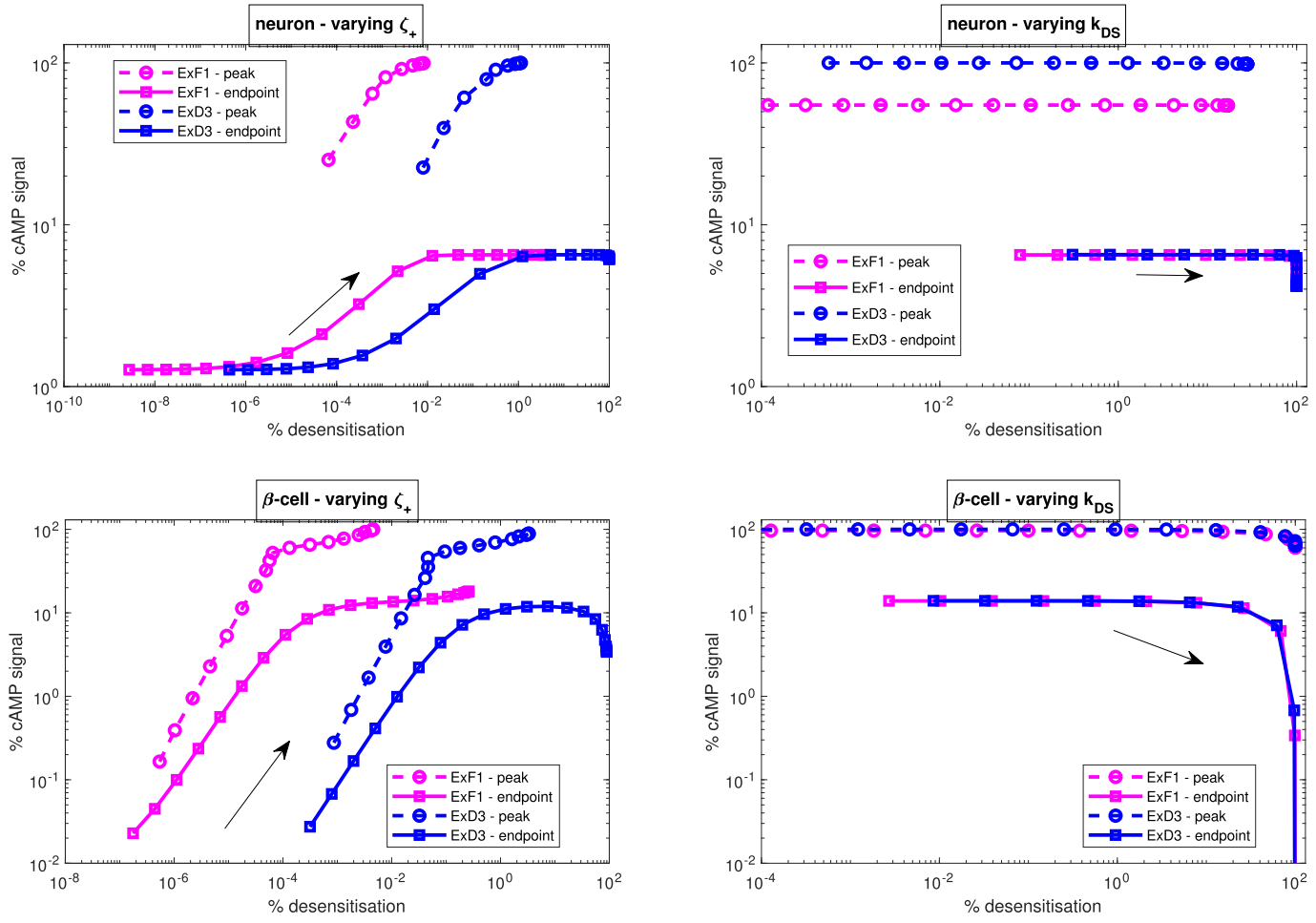

Fig. 18. Simulated effect of ligand efficacy parameter ζ_+ or k_{DS} on cAMP response and desensitisation in both neurons and β-cells, for both ligands, each for ligand concentration $[L] = 100$nM. The arrow in each plot shows indicates the direction along the curve in which the parameter value is increasing.

parameter ζ_+ (which is specific to the ligand) on cAMP timecourses and their peak and endpoint (60 mins) signals. With ζ_- fixed in each simulation, increasing ζ_+ increases the both the ligand-bound activation rate and the equilibrium propensity for ligand-bound receptor activation, or the level of agonism. Over the range of values shown, we see that the peak response increases monotonically with ζ_+, as expected. In β-cells, the peak response is maintained throughout, but for low values of ζ_+, there is no peak response in neurons. The endpoint response is monotonic in both cell types for ExF1 only; the response to ExD3 is non-monotonic, and markedly so for β-cells. At higher values of ζ_+, the endpoint signal decreases as the response to ExD3 is more transient than that for ExF1.

We further explore the competing effects of desensitisation and receptor-mediated signalling in Figs. 18–19. In [23], both a GPCR signalling model response and theoretical receptor desensitisation percentage are computed as efficacy and desensitisation parameters are varied independently. Fig. 18 shows a corresponding analysis for our cAMP model. In agreement with [23], increasing k_{DS} increases desensitisation and decreases the signal in each case, while increasing ζ_+ increases both the signal and the desensitisation level at the endpoint. We conclude that ligands with higher efficacy values ζ_+ will increase the signal as expected, but also lead to an increase in the competing effect of receptor desensitisation. We observe the non-monotonicity in the peak response as a function of ζ_+ for β-cells again.

Response surfaces are popular for visualising effects of competing processes and multi-parameter sensitivity studies [2,4,5]. In Fig. 19, we show response surfaces for parameters ζ_+ and k_{DS}. The monotonicity for the peak signal and potential non-monotonicity for the endpoint signal with respect to ζ_+ are evident. The signals with the greatest sensitivity to the two parameters about the estimated values are those for β-cells.

6. Discussion

In this paper, we have formulated a mathematical model to enable qualitative and quantitative insights into the potential downstream signalling kinetics induced by two GLP1-R agonists in both β-cells and neurons. The model is based on a G protein-coupled receptor binding and activation schematic, with a receptor desensitisation module and second messenger (cAMP) generation. We have particularly focused on the binding, activation and desensitisation sub-model detail such that the signalling trade-off between pathway activation and desensitisation can be addressed. The model has been parameterised first using HEK293 cells, to estimate ligand on and off rates, then for experimental data for β-cells and neurons.

The data fitting shows that the model supports a parameterisation whereby the peak cAMP responses for ExF1 and ExD3 are similar in β-cells with more pronounced drop for ExD3, and a lower peak cAMP response for ExF1 in neurons, with the long-time cAMP signals similar. Simulations beyond the duration of the experiment in each case suggest that the cAMP response for both ligands in neurons has reached a pseudo-steady state on the timescale of the experiment. In contrast, the simulated long-time responses to the two ligands in β-cells are significantly different; the ExF1 response is at an apparent steady-state, but the ExD3 continues to decay and is negligible at around 8 h. This finding adds support to the hypothesis that ExF1 offers more potential glucose regulation benefit than ExD3 over long timescales via signalling in pancreatic β-cells, but that there is little difference between the two ligands in the potential appetite suppression effects offered via long-time signalling in neurons on the same timescales.

Ligand concentration and total receptor are predicted to have significant effect on the cAMP responses. In particular, at low ligand concentrations, the peak-plateau nature of the signalling kinetics is not maintained, and a monotonic cAMP timecourse is observed. Receptor desensitisation is a key factor in both peak and plateau responses where they exist. For neurons, both ligands of interest give a simulated apparent non-zero steady-state cAMP response, even for large desensitisation rates. In contrast, for β-cells, large desensitisation rates result in pronounced drop-off in long-time response for both ligands of interest. Rechallenge simulations and tracking of the desensitised receptor proportion have been used to illustrate and understand the potential desensitisation effect. It is clear that ExF1-occupied receptor experiences a much lower level of desensitisation than ExD3-occupied receptor in both cell types, and for β-cells, this corresponds with the long-time

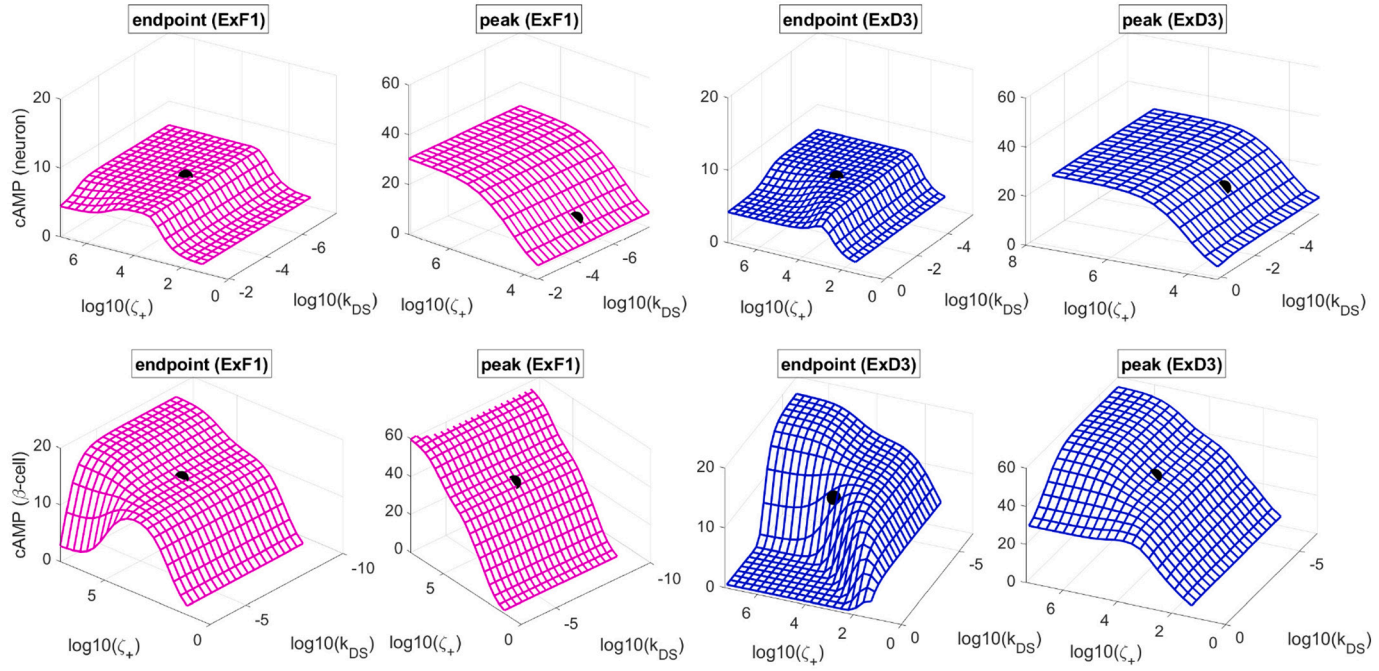

Fig. 19. Simulated effect of ligand efficacy parameter ζ_+ and k_{DS} on cAMP response in both neurons and β-cells, for both ligands, each for ligand concentration $[L]$ = 100nM. Top panel (neuron simulations) - cAMP response surfaces for both ligands, for peak and endpoint (60 min) signals. Bottom panel (β-cell simulations) - as above. The circle on each surface indicates the estimated values of ζ_+ and k_{DS} from Fig. 5.

sustained cAMP signal observed for ExF1. The cAMP signal is seen to depend on both the ligand efficacy parameter ζ_+ and the desensitisation constant k_{DS}, which are both ligand-dependent. The monotonicity of the dependence on ζ_+ is itself dependent on the time at which the cAMP reading is taken. Our analysis clearly demonstrates the potential for a kinetic context for different activation-desensitisation trade-off effects; parameter sensitivity results are different at different timepoints.

The excellent data fitting suggests that our model may be useful for parameterising and understanding signalling in different cells, driven by different ligands. While our analysis focuses largely on ligand/receptor-level signal generation and modulation, more detailed analysis of the cAMP pathway would be possible if insights into cAMP signalling cascade components based on pathway readouts were required [26]. Our model could also be extended to consider the role of β-arrestin in desensitisation explicitly, using further schematics from [26]. Following the approaches of [3,26], we have analysed our model by using numerical simulations only. Our results indicate that the cAMP signalling cascade evolves on multiple timescales. As such, asymptotic analysis could be used to elucidate the signal transduction dynamics in detail [2,4], but this is beyond our scope here.

Another model extension that we propose as future work is to include the effects of receptor internalisation. GLP-1R is known to internalise into endosomes, and with further data we may be able to quantify the potentially different extents of internalisation between the two ligands ExF1 and ExD3. Internalisation and other membrane trafficking processes are predicted to modulate cAMP signalling via several mechanisms. For example, bulk sequestration of the receptor away from the plasma membrane will reduce access of extracellular ligand to available cell surface receptor, whilst at the same time promoting distinct cAMP signalling networks from the endosomal compartment [29]. Mathematical models for internalisation in varying degrees of detail are available in the literature [8,30–33].

We remark that extension of the current model to include arrestin recruitment and receptor internalisation will increase the order of the ODE system and further challenge its analytical tractability. However, the use of an ODE model and its requirement for numerical solution is warranted; the popular operational model of agonism [34] is based on equilibrium assumptions and an empirical sub-model which preclude both kinetic and mechanistic insights and associated parameterisations for our GLP-1R-cAMP system. Recently proposed kinetic operational models comprise low-dimensional ODE systems for signal transduction based on equilibrium ligand binding assumptions [7,25] as kinetic alternatives to the original equilibrium model [34]. An active field of theoretical research, beyond our scope here, involves the application of model reduction techniques to detailed ODE models of cell signalling [35] which may help to bridge the gap between systems biology-type models and operational models.

Our analysis suggests that ExD3 is more "biased" towards receptor desensitisation than ExF1 is, without explicitly defining a measure of biased agonism. Future work which considers a model of β-arrestin signalling versus G protein activation (see [14–16,26]) will explicitly quantify the dynamic "ligand bias" [3,36] associated with multiple signalling responses (using definitions from [3]), to further characterise ExF1 and ExD3 effects in different cell types within the context of biased therapeutics [36,37]. Furthermore, we will consider the structural identifiability properties of the governing system in future work [38].

The agonists used in this work, ExF1 and ExD3, were selected as tool compounds to probe the impact of their distinct signalling properties. However, the findings may be of therapeutic relevance because of the current interest in potential differences between clinically approved ligands showing balanced (e.g. semaglutide) versus G protein-biased (e.g. tirzepatide) GLP-1R agonism. As the receptor pharmacology of ExD3 resembles the former and ExF1 the latter, it may be reasonable to ask whether the findings in our work inform better understanding of the therapeutic profile of these major GLP-1R-based agents. From our data, we might predict that G protein-biased agonists would accentuate β-cell-mediated (e.g. blood glucose lowering) more than neuronally-mediated (e.g. appetite suppression, nausea) effects. This possibility requires experimental validation but, if confirmed, might guide development of GLP-1R and other GPCR agonists with more selective pharmacodynamic profiles.

CRediT authorship contribution statement

Lloyd Bridge: Formal analysis, Investigation, Methodology, Writing – original draft. **Shiqian Chen:** Data curation. **Ben Jones:** Writing – original draft, Project administration, Methodology, Investigation, Conceptualization, Data curation.

Declaration of competing interest

The authors declare that they have no known competing financial interests or personal relationships that could have appeared to influence the work reported in this paper.

Data availability

Data will be made available on request.

Acknowledgements

LB was supported in part by a College of Arts, Technology and the Environment funding award at UWE Bristol. BJ is supported by an MRC Clinician Scientist Fellowship (MR/Y00132X/1), as well as project grants from the MRC, EFSD and Diabetes UK. The Section of Endocrinology at Imperial College London is funded by grants from the MRC, NIHR and is supported by the NIHR Biomedical Research Centre Funding Scheme and the NIHR/Imperial Clinical Research Facility. The views expressed are those of the author(s) and not necessarily those of the NHS, the NIHR or the Department of Health.

Appendix A. Experimental methods

A.1. Cell lines and cell culture

Adherent HEK293 cells (AD293) were cultured in DMEM supplemented with 10% foetal bovine serum (FBS) and 1% penicillin/streptomycin.

A.2. Animals

Animal procedures at Imperial College London were approved by the British Home Office under the UK Animals (Scientific Procedures) Act 1986. Mice (Charles River, UK) were group housed and held in a condition-controlled room at 21–23 °C with 12 h:12 h light to dark cycles (lights on at 07:00). All animals had ad libitum access to water and feed. Lean mice were fed standard chow (RM1(E); Special Diet Services, UK). CAMPER mice were obtained from Jackson laboratories (C57BL/6-*Gt*(*ROSA*)26*Sor*$^{tm1(CAG-ECFP^*/Rapgef3/Venus)Kama}$/J, Jax strain #032205). These mice encode the cAMP FRET reporter ^{T}Epac^{VV} flanked by a STOP-flox in the ROSA26 locus, allowing tissue specific expression when bred with appropriate Cre-expressing

strains. In this study, we used β-actin-Cre mice (B6N.FVB-*Tmem*163$^{Tg(ACTB-cre)2Mrt}$/CjDswJ, Jax strain #019099) to achieve global ^{T}Epac^{VV} expression in all tissues, *Pdx1*-Cre-ERT (STOCK Tg(Pdx1-cre/Esr1*)#Dam/J, Jax strain #024968) for β-cell-specific expression. These mice are referred to as CAMPER^{ACTB} and CAMPER$^{Pdx1\text{-}ERT}$, respectively. For CAMPER$^{Pdx1\text{-}ERT}$ experiments, ^{T}Epac^{VV} expression was induced in vitro (after tissue isolation) using 200 nM 4-hydroxytamoxifen (4-OHT) for 24 h before imaging.

A.3. Isolation, dispersal and culture of pancreatic islets

CAMPER$^{Pdx1\text{-}ERT}$ mice were culled by cervical dislocation and positioned with the abdomen facing upwards. After skin was sterilized using 70% ethanol, an incision was made around the upper abdomen to expose the pancreas and common bile duct. Pancreata were inflated with RPMI-1640 medium (R8758, Sigma-Aldrich) containing 1 mg/ml collagenase from *Clostridium histolyticum* (S1745602, Nordmark Biochemicals), dissected and incubated in a water-bath at 37 °C for 12 min. Islets were subsequently washed and purified using a Histopaque gradient (Histopaque-1119, 11,191, Sigma-Aldrich, and Histopaque-1083, 10,831, Sigma-Aldrich). Isolated islets were allowed to recover overnight in RPMI-1640 supplemented with 10% *v*/v FBS (F7524, Sigma-Aldrich) and 1% v/v Penicillin-Streptomycin solution (15070–063, Invitrogen). To induce ^{T}Epac^{VV} expression, islets were treated with 200 nM 4-hydroxytamoxifen (4-OHT). The morning after isolation, islets were dispersed into single cells by gentle trituration in 0.05% trypsin-EDTA for 3 min. Dispersed islet cells were seeded onto black 96-well microplates coated with mg/ml poly-D-lysine and 20 μg/ml laminin for 24 h before the assay.

A.4. Isolation and culture of nodose ganglion neurons

Nodose ganglia from CAMPER^{ACTB} mice were dissected and placed in 500 μl extraction buffer, i.e. HEPES-buffered Kreb's-Ringer Bicarbonate buffer (KCl 4.7 mM, KH_2PO_4 1.2 mM, NaCl 129 mM, $NaHCO_3$ 5 mM, $MgSO_4$ 1.2 mM, $CaCl_2$ 1.8 mM, HEPES 10 mM, glucose 5.6 mM, pH 7.4) containing 22 μl 2.5 mg/ml liberase for 45 min at 37 °C. The resulting suspension was pelleted and washed twice with PBS, resuspended in full medium (Neurobasal plus 2% B27, 1% L-glutamine, 1% FBS, 0.05% NGF), followed by trituration and passage through a 70 μM filter to remove debris. The resulting cell suspension was seeded onto glass bottomed petri dishes coated with 0.1 mg/ml poly-D-lysine and laminin 20 μg/ml and cultured in full medium for 24–48 h before experiments.

A.5. Monitoring cAMP responses in transiently transduced AD293 cells

AD293 cells were seeded in black 96-well plates (30,000 cells/well) coated with 0.01% poly-D-lysine and transduced for 24 h with the "green up" cADDis cAMP sensor (Montana Molecular, USA, 15 μl/well) according to the manufacturer's instructions. hGLP-1R in a BacMam vector (Montana Molecular, 10 μl/well) was also transduced at specified times before the stimulation step (8, 6, 4 and 2 h) to achieve varying GLP-1R densities. Timings were selected so that agonist-stimulated cAMP responses remained within the dynamic range of the sensor. Media was removed from the cells and replaced with HBSS containing 0.1% BSA. Fluorescence signal (λ_{ex} = 485 nm, λ_{em} = 525 nm) was recorded before and after addition of agonist at a maximal concentration (1 μM) by the automated pipette in a Flexstation 3 instrument. Readings were taken every 2 s. Positive control wells received IBMX (500 μM) plus FSK (50 μM) as a maximal stimulus to indicate the sensor saturation point. Signal change was first expressed as fractional change from baseline, followed by subtraction of the signal trace from negative control wells (no GLP-1R expressed) to account for sensor photobleaching.

A.6. Determination of surface GLP-1R concentrations in transiently transduced AD293 cells

AD293 cells in poly-D-lysine-coated black walled, clear bottom 96-well plates (30,000 cells/well) were transduced with hGLP1R in parallel at the same time as those used for cADDis experiments. To quantify relative GLP-1R density, cells were treated with Cy5-tagged exendin-4 [39], which labels GLP-1R at the cell surface before undergoing internalisation, for 30 min before washing and then imaging by fluorescence microscopy. A modified Nikon Ti2E with automated stage was used to acquire several epifluorescence and transmitted light phase contrast fields-of-view (FOVs) from each well. Cell-associated Cy5 intensity, indicating ligand-bound GLP-1R, was analysed by applying a flat-field correction and segmentation of cell-containing regions using Phantast [40].

A.7. Experimental assessment of agonist binding kinetics

The assay was performed as previously described [15]. HEK293 cells stably expressing N-terminal SNAP-tagged hGLP1R were labelled with 40 nM Lumi4-Tb (Cisbio, France) for 30 min at 4 °C, including a metabolic inhibitor cocktail (10 mM NaN_3, 20 mM 2-deoxyglucose) to inhibit GLP-1R internalisation. After washing, TR-FRET was monitored using a Flexstation 3 plate reader on simultaneous addition of unlabelled agonist plus 10 nM exendin-4-FITC. Association and dissociation rate constants were calculated using the kinetics of competitive binding algorithm in GraphPad Prism.

A.8. Monitoring cAMP responses in dispersed islets and nodose ganglion neurons

Dispersed islets from CAMPER$^{Pdx1\text{-}ERT}$ mice, and nodose ganglion cultures from CAMPER^{ACTB} mice were prepared as above. For imaging, cells were gently washed and placed in Kreb's-Ringer bicarbonate HEPES (KRBH) buffer (140 mM NaCl, 3.6 mM KCl, 1.5 mM $CaCl_2$, 0.5 mM $MgSO_4$, 0.5 mM NaH_2PO_4, 2 mM $NaHCO_3$, 10 mM HEPES, saturated with 95% O_2/5% CO_2; pH 7.4) containing 0.1% BSA and 6 mM glucose. Imaging was performed using an image splitter (Cairn OptoSplit III) inserted in the optical path to simultaneously acquire images in CFP and YFP channels. Typically, hundreds of cells were imaged per condition. Cells were imaged before and for 60 min after addition of agonist at a maximal concentration (100 nM) or vehicle. A positive control stimulus containing 500 μM isobutylmethylxanthine (IBMX) and 50 μM forskolin (FSK) was then added for 5 min to saturate the sensor. Image analysis was performed using custom macros in ImageJ v1.54f. First, drift correction was applied using SIFT and flatfield illumination correction in each channel using BaSiC [41]. A maximum intensity projection of the time series was used to segment cells, from which the YFP/CFP FRET signal was determined at each timepoint. Non-cell objects and dead cells were excluded according to IBMX/FSK response. The mean

response from all cells was determined, with normalisation to baseline and to IBMX/FSK applied.

Appendix B. Parameter values

Table 4
Estimated parameter values for Sections 4–5.

Parameter	Value	Cell A (neuron)	Cell B (islet)	Ligand 1 (ExF1)	Ligand 2 (ExD3)	Units
k_{L-}	0.2485	✓	✓	✓		s^{-1}
k_{L-}	0.0134	✓	✓		✓	s^{-1}
k_{L+}	2.233×10^{7}	✓	✓	✓		$M^{-1}\,s^{-1}$
k_{L+}	1.922×10^{7}	✓	✓		✓	$M^{-1}\,s^{-1}$
k_{act+}	0.0015	✓		✓	✓	s^{-1}
k_{act+}	0.2438		✓	✓	✓	s^{-1}
k_{act-}	347.67	✓		✓	✓	s^{-1}
k_{act-}	1.790×10^{4}		✓	✓	✓	s^{-1}
k_{G+}	4.726×10^{6}	✓		✓	✓	$M\,s^{-1}$
k_{G+}	7.780×10^{4}		✓	✓	✓	$M\,s^{-1}$
k_{G-}	5.103×10^{-6}	✓		✓	✓	s^{-1}
k_{G-}	0.0289		✓	✓	✓	s^{-1}
δ_{+}	0.0390	✓		✓		–
δ_{+}	0.0311	✓			✓	–
δ_{+}	5.702×10^{-5}		✓	✓		–
δ_{+}	1.486×10^{-16}		✓		✓	–
δ_{-}	1.885×10^{-4}	✓		✓		–
δ_{-}	1.944×10^{-4}	✓			✓	–
δ_{-}	2.1474×10^{-14}		✓	✓		–
δ_{-}	2.552×10^{-9}		✓		✓	–
$\zeta +$	1.2346×10^{4}	✓	✓	✓		–
$\zeta +$	2.2611×10^{4}	✓	✓		✓	–
$\zeta -$	1.8551	✓	✓	✓		–
$\zeta -$	0.9776	✓	✓		✓	–
$\mu +$	0.5206	✓		✓	✓	–
$\mu +$	1.9944		✓	✓	✓	–
$\mu -$	0.0345	✓		✓	✓	–
$\mu -$	0.0384		✓	✓	✓	–
k_{GTP+}	0.0144	✓		✓	✓	s^{-1}
k_{GTP+}	0.0993		✓	✓	✓	s^{-1}
k_{DS}	1.299×10^{-5}	✓		✓		s^{-1}
k_{DS}	0.0018	✓			✓	s^{-1}
k_{DS}	7.418×10^{-7}		✓	✓		s^{-1}
k_{DS}	6.341×10^{-4}		✓		✓	s^{-1}
ν_{+}	0.9390	✓		✓		–
ν_{+}	2.5825	✓			✓	–
ν_{+}	0.8674		✓	✓		–
ν_{+}	0.7571		✓		✓	–
ν_{-}	0.9644	✓		✓		–
ν_{-}	0.9597	✓			✓	–
ν_{-}	0.1696		✓	✓		–
ν_{-}	0.1683		✓		✓	–
θ_{a}	0.8668	✓		✓	✓	–
θ_{a}	4.2125		✓	✓	✓	–
k_{RA+}	8.213×10^{3}	✓		✓	✓	$M^{-1}s^{-1}$
k_{RA+}	2.029×10^{6}		✓	✓	✓	$M^{-1}s^{-1}$
k_{RA-}	3.144×10^{-19}	✓		✓	✓	$M^{-1}s^{-1}$
k_{RA-}	6.516×10^{-19}		✓	✓	✓	$M^{-1}s^{-1}$
k_{hyd+}	0.1393	✓		✓	✓	s^{-1}
k_{hyd+}	0.0634		✓	✓	✓	s^{-1}
k_{hyd-}	9.126×10^{-4}	✓		✓	✓	s^{-1}
k_{hyd-}	2.492×10^{-15}		✓	✓	✓	s^{-1}
k_{cAMP+}	0.1236	✓		✓	✓	s^{-1}
k_{cAMP+}	4.8893		✓	✓	✓	s^{-1}
k_{cAMP-}	0.0964	✓		✓	✓	s^{-1}
k_{cAMP-}	0.1268		✓	✓	✓	s^{-1}
R_{tot}	6.591×10^{-10}	✓		✓	✓	M
R_{tot}	6.648×10^{-9}		✓	✓	✓	M
G_{tot}	1.405×10^{-9}	✓		✓	✓	M
G_{tot}	2.231×10^{-10}		✓	✓	✓	M
a	5.518×10^{11}	✓	✓	✓	✓	–

References

[1] Vicent Casadó, Verònica Casadó-Anguera, What are the current trends in g protein-coupled receptor targeted drug discovery? Expert Opin. Drug Discovery (2023) 1–6.

[2] L.J. Bridge, J.R. King, S.J. Hill, M.R. Owen, Mathematical modelling of signalling in a two-ligand g-protein coupled receptor system: agonist–antagonist competition, Math. Biosci. 223 (2) (2010) 115–132.

[3] L.J. Bridge, Jack Mead, Eugenia Frattini, Ian Winfield, Graham Ladds, Modelling and simulation of biased agonism dynamics at a g protein-coupled receptor, J. Theor. Biol. 442 (2018) 44–65.

[4] P.J. Woodroffe, L.J. Bridge, J.R. King, S.J. Hill, Modelling the activation of g-protein coupled receptors by a single drug, Math. Biosci. 219 (1) (2009) 32–55.

[5] P.J. Woodroffe, L.J. Bridge, J.R. King, C.Y. Chen, S.J. Hill, Modelling of the activation of g-protein coupled receptors: drug free constitutive receptor activity, J. Math. Biol. 60 (3) (2010) 313–346.

[6] Carla White, Lloyd J. Bridge, Ligand binding dynamics for pre-dimerised g protein-coupled receptor homodimers: linear models and analytical solutions, Bull. Math. Biol. 81 (9) (2019) 3542–3574.

[7] Samuel R.J. Hoare, Nicolas Pierre, Arturo Gonzalez Moya, Brad Larson, Kinetic operational models of agonism for g-protein-coupled receptors, J. Theor. Biol. 446 (2018) 168–204.

[8] James A. Adams, Geneva M. Omann, Jennifer J. Linderman, A mathematical model for ligand/receptor/g-protein dynamics and actin polymerization in human neutrophils, J. Theor. Biol. 193 (4) (1998) 543–560.

[9] Timo D. Müller, S.R. Brian Finan, David D'Alessio Bloom, Daniel J. Drucker, P. R. Flatt, A. Fritsche, H.J. Fiona Gribble, J.F. Habener Grill, et al., Glucagon-like peptide 1 (glp-1), Molecular metabolism 30 (2019) 72–130.

[10] Daniel J. Drucker, Mechanisms of action and therapeutic application of glucagon-like peptide-1, Cell Metab. 27 (4) (2018) 740–756.

[11] Mette Q. Ludwig, Wenwen Cheng, Desiree Gordian, Julie Lee, Sarah J. Paulsen, Stine N. Hansen, Kristoffer L. Egerod, Pernille Barkholt, Christopher J. Rhodes, Anna Secher, et al., A genetic map of the mouse dorsal vagal complex and its role in obesity, Nature Metabolism 3 (4) (2021) 530–545.

[12] Alejandra Tomas, Ben Jones, Colin Leech, New insights into beta-cell glp-1 receptor and camp signaling, J. Mol. Biol. 432 (5) (2020) 1347–1366.

[13] Amaara Marzook, Alejandra Tomas, Ben Jones, The interplay of glucagon-like peptide-1 receptor trafficking and signalling in pancreatic beta cells, Front. Endocrinol. 12 (2021) 678055.

[14] Hongkai Zhang, Emmanuel Sturchler, Jiang Zhu, Ainhoa Nieto, Philip A. Cistrone, Jia Xie, LinLing He, Kyungmoo Yea, Teresa Jones, Rachel Turn, et al., Autocrine selection of a glp-1r g-protein biased agonist with potent antidiabetic effects. Nature, Communications 6 (1) (2015) 8918.

[15] Ben Jones, Teresa Buenaventura, Nisha Kanda, Pauline Chabosseau, Bryn M. Owen, Rebecca Scott, Robert Goldin, Napat Angkathunyakul, Ivan R. Corrêa Jr, Domenico Bosco, et al., Targeting glp-1 receptor trafficking to improve agonist efficacy, Nat. Commun. 9 (1) (2018) 1602.

[16] Maria Lucey, Philip Pickford, Stavroula Bitsi, James Minnion, Jan Ungewiss, Katja Schoeneberg, Guy A. Rutter, Stephen R. Bloom, Alejandra Tomas, Ben Jones, Disconnect between signalling potency and in vivo efficacy of pharmacokinetically optimised biased glucagon-like peptide-1 receptor agonists, Molecular Metabolism 37 (2020) 100991.

[17] Francis S. Willard, Jonathan D. Douros, Maria B.N. Gabe, Aaron D. Showalter, David B. Wainscott, Todd M. Suter, Megan E. Capozzi, Wijnand J.C. van der Velden, Cynthia Stutsman, Guemalli R. Cardona, et al., Tirzepatide is an imbalanced and biased dual gip and glp-1 receptor agonist, JCI Insight 5 (17) (2020).

[18] Takahiro Kawai, Bingfa Sun, Hitoshi Yoshino, Dan Feng, Yoshiyuki Suzuki, Masanori Fukazawa, Shunsuke Nagao, David B. Wainscott, Aaron D. Showalter, Brian A. Droz, et al., Structural basis for glp-1 receptor activation by ly3502970, an orally active nonpeptide agonist, Proceedings of the National Academy of Sciences 117 (47) (2020) 29959–29967.

[19] Phil Pickford, Maria Lucey, Roxana-Maria Rujan, Emma Rose McGlone, Stavroula Bitsi, Fiona B. Ashford, Ivan R. Corrêa, David J. Hodson, Alejandra Tomas, Giuseppe Deganutti, et al., Partial agonism improves the anti-hyperglycaemic efficacy of an oxyntomodulin-derived glp-1r/gcgr co-agonist, Molecular Metabolism 51 (2021) 101242.

[20] Paul Richards, Helen E. Parker, Alice E. Adriaenssens, Joshua M. Hodgson, Simon C. Cork, Stefan Trapp, Fiona M. Gribble, Frank Reimann, Identification and characterization of glp-1 receptor–expressing cells using a new transgenic mouse model, Diabetes 63 (4) (2014) 1224–1233.

[21] Julia Ast, Johannes Broichhagen, David J. Hodson, Reagents and models for detecting endogenous glp1r and gipr, EBioMedicine 74 (2021).

[22] Tamara L. Kinzer-Ursem, Jennifer J. Linderman, Both ligand-and cell-specific parameters control ligand agonism in a kinetic model of g protein–coupled receptor signaling, PLoS Comput. Biol. 3 (1) (2007) e6.

[23] Todd A. Riccobene, Geneva M. Omann, Jennifer J. Linderman, Modeling activation and desensitization of g-protein coupled receptors provides insight into ligand efficacy, J. Theor. Biol. 200 (2) (1999) 207–222.

[24] Liliana R.V. Castro, Elvire Guiot, Marina Polito, Daniéle Paupardin-Tritsch, Pierre Vincent, Decoding spatial and temporal features of neuronal camp/pka signaling with fret biosensors, Biotechnol. J. 9 (2) (2014) 192–202.

[25] Sam R.J. Hoare, Paul H. Tewson, Anne Marie Quinn, Thomas E. Hughes, Lloyd J. Bridge, Analyzing kinetic signaling data for g-protein-coupled receptors, Sci. Rep. 10 (1) (2020) 12263.

[26] Jonathan D. Violin, Lisa M. DiPilato, Necmettin Yildirim, Timothy C. Elston, Jin Zhang, Robert J. Lefkowitz, β2-adrenergic receptor signaling and desensitization elucidated by quantitative modeling of real time camp dynamics, J. Biol. Chem. 283 (5) (2008) 2949–2961.

[27] Rachel Vistein, Manojkumar A. Puthenveedu, Reprogramming of g protein-coupled receptor recycling and signaling by a kinase switch, Proceedings of the National Academy of Sciences 110 (38) (2013) 15289–15294.

[28] Wenkuan Xin, Tuan M. Tran, Wito Richter, Richard B. Clark, Thomas C. Rich, Roles of grk and pde4 activities in the regulation of β2 adrenergic signaling, J. Gen. Physiol. 131 (4) (2008) 349–364.

[29] Jean-Pierre Vilardaga, Frederic G. Jean-Alphonse, Thomas J. Gardella, Endosomal generation of camp in gpcr signaling, Nat. Chem. Biol. 10 (9) (2014) 700–706.

[30] Douglas A. Lauffenburger, Jennifer Linderman, Receptors: Models for Binding, Trafficking, and Signaling, Oxford University Press, 1993.

[31] Abraham R. Tzafriri, Wu David, Elazer R. Edelman, Analysis of compartmental models of ligand-induced endocytosis, J. Theor. Biol. 229 (1) (2004) 127–138.

[32] H. Harish Shankaran, Steven Wiley, Haluk Resat, Receptor downregulation and desensitization enhance the information processing ability of signalling receptors, BMC Syst. Biol. 1 (1) (2007) 1–15.

[33] Mostafa Maalmi, William Strieder, Arvind Varma, Ligand diffusion and receptor mediated internalization: Michaelis–menten kinetics, Chem. Eng. Sci. 56 (19) (2001) 5609–5616.

[34] James Whyte Black, Paul Leff, Operational models of pharmacological agonism, Proceedings of the Royal society of London. Series B. Biological sciences 220 (1219) (1983) 141–162.

[35] Thomas J. Snowden, Piet H. van der Graaf, Marcus J. Tindall, Methods of model reduction for large-scale biological systems: a survey of current methods and trends, Bull. Math. Biol. 79 (2017) 1449–1486.

[36] Dylan Scott Eiger, Uyen Pham, Julia Gardner, Chloe Hicks, Sudarshan Rajagopal, Gpcr systems pharmacology: a different perspective on the development of biased therapeutics, American Journal of Physiology-Cell Physiology 322 (5) (2022) C887–C895.

[37] H. Ongun Onaran, Tommaso Costa, Conceptual and experimental issues in biased agonism, Cell. Signal. 82 (2021) 109955.

[38] Carla White, Vivi Rottschäfer, and Lloyd Bridge., Classical structural identifiability methodology applied to low-dimensional dynamic systems in receptor theory, J. Pharmacokinet. Pharmacodyn. (2023) 1–25.

[39] Zijian Fang, Shiqian Chen, Yusman Manchanda, Stavroula Bitsi, Philip Pickford, Alessia David, Maria M. Shchepinova, Ivan R. Corrêa Jr, David J. Hodson, Johannes Broichhagen, et al., Ligand-specific factors influencing glp-1 receptor post-endocytic trafficking and degradation in pancreatic beta cells, Int. J. Mol. Sci. 21 (21) (2020) 8404.

[40] Nicolas Jaccard, Lewis D. Griffin, Ana Keser, Rhys J. Macown, Alexandre Super, Farlan S. Veraitch, Nicolas Szita, Automated method for the rapid and precise estimation of adherent cell culture characteristics from phase contrast microscopy images, Biotechnol. Bioeng. 111 (3) (2014) 504–517.

[41] T. Peng, K. Thorn, T. Schroeder, L. Wang, F.J. Theis, C. Marr, N. Navab, A basic tool for background and shading correction of optical microscopy images, Nat. Commun. 8 (2017) 14836.